Chemical Engineering Science xxx (xxxx) xxx

Contents lists available at ScienceDirect

Chemical Engineering Science

journal homepage: www.elsevier.com/locate/ces

Modelling of gas injection into a viscous liquid through a top-submerged lance

Yannan Wang [a,*], Lingling Cao [a], Maarten Vanierschot [b], Zhongfu Cheng [a], Bart Blanpain [a], Muxing Guo [a]

[a] Department of Materials Engineering, KU Leuven, 3000 Leuven, Belgium
[b] Mechanical Engineering Technology Cluster TC, Campus Group T Leuven, KU Leuven, 3000 Leuven, Belgium

HIGHLIGHTS

- The VOF-LES-DSL model predicts the turbulent top-submerged lance flow well.
- 3D simulation is indispensable for capturing flow fluctuations.
- The flow characteristics are quantitatively described under industrial conditions.

ARTICLE INFO

Article history:
Received 16 May 2019
Received in revised form 11 November 2019
Accepted 15 November 2019
Available online xxxx

Keywords:
Top injection flow
Viscous liquid
VOF-RNG/LES
Subgrid scale model
Model validation
Flow characteristics

ABSTRACT

The hydrodynamics of a gas-viscous liquid flow is numerically studied by coupling the Volume of Fluid (VOF) method with the Renormalization Group (RNG) k-ε model or Large Eddy Simulation (LES) (VOF-RNG or VOF-LES). The simulations are validated by Particle Imaging Velocimetry (PIV) measurements. Averaged flow features are predicted by 2D and 3D VOF-RNG/LES models. Only the 3D VOF-LES model predicts the velocity fluctuation well. The Dynamic Smagorinsky-Lilly (DSL) Subgrid-scale model slightly outperforms the Wall-Adapting Local Eddy-Viscosity (WALE) subgrid-scale model. Subsequently, flow characteristics of a gas-viscous liquid flow are studied by the validated 3D VOF-LES-DSL model under industrially relevant conditions. Gas penetration depth, flow velocity attenuation, surface sloshing and slag splashing are quantitatively described. The flow regime is identified through the pressure data monitored in the lance and its Fast Fourier Transform (FFT) results. The study of the coherent structures shows strong vortices in the top part of the slag pot.

1. Introduction

Currently, about 10 million tons of Basic Oxygen Furnace (BOF) slag is annually produced as a main by-product during the steel-making process in Europe (Euroslag). Therefore, the reuse/recycling of BOF slag becomes a very urgent issue since it causes land occupation for slag disposal, environmental issues and a waste of precious resources (Dippenaar, 2005). However, BOF slag valorization is restricted by its volume swelling during natural aging due to the presence of free lime (Mikhail and Turcotte, 1995; Wang et al., 2010). In order to solve this problem, the FEhS Institute has developed and implemented a process, where silica-rich additives are injected into the liquid slag with nitrogen or oxygen as a carrier gas through a top submerged lance for the stabilization of free lime at high temperature (Motz and Geiseler, 2001; Santos et al., 2012). As a consequence, a flow in the slag pot is generated by the materials' (*i.e.*, the mixture of silica-rich additives and carrier gas) injection, during which the buoyancy of the injected gas phase has a major influence on the flow formation. Therefore, it is reasonable to simplify this system as a gas–liquid two-phase flow to study the influence of the flow on the additives movement and the mass transport, which directly affects the additive dissolution during the process.

Due to difficulties of high temperature experiments (*e.g.*, opacity of a slag pot, hazardous operating environment, lack of velocity measuring techniques at high temperature), physical modelling (Igwe et al., 1973; Mazumdar and Guthrie, 1985; Iguchi et al., 1994; Morsi et al., 2000; Zhao et al., 2016, 2017; Pan and Langberg, 2010) and numerical simulation (Mazumdar and Guthrie, 1985; Liovic et al., 2002; Huda et al., 2010, 2012; Wang et al., 2018; Sattar et al., 2014; Obiso et al., 2019) have been performed on a top injection two-phase flow in a metallurgical vessel. Iguchi et al. (1994) performed some cold model experiments to analyze the fluid flow initiated by the top submerged gas injection

* Corresponding author.
E-mail address: yannan.wang@kuleuven.be (Y. Wang).

https://doi.org/10.1016/j.ces.2019.115359
0009-2509/

Nomenclature

a	average radius of the slag pot, m
A	cross-section area of lance, m^2
$C_{1\varepsilon}, C_{2\varepsilon}$	model constants, 1.42, 1.68, respectively
$C_{3\varepsilon}$	model constant
C_s	model constant
d_L	lance diameter, m
d_n	nozzle diameter, m
D_P	penetration depth, m
E_{In}	input energy flux accompanied with the gas phase, kJ/(m^2·s)
E_{ke}	power input from gas kinetic energy, W
f	frequency, Hz
F_{csf}	surface tension, N
Fr_m	modified Froude number
H_c	characteristic length, m
g	gravitational acceleration, m/s^2
G_b	turbulence generation due to buoyancy, kg/(m·s^3)
G_k	turbulence generation due to the mean velocity gradient, kg/(m·s^3)
k	turbulent kinetic energy, m^2/s^2
k_i	the ith root of the derivative of the first-order Bessel function, $J_1'(k_i) = 0$
K	curvature, 1/m
l	submerged lance depth, m
L	liquid level, m
Δm	loss of the molten slag, kg
m	the amount of slag in the slag pot, 55740 kg
M_l	angular momentum of the liquid slag, kg·m^2/s
M_o	angular momentum of the slag pot, kg·m^2/s
n	phase number
$\dot{n}$	molar flowrate, mol/s
p	pressure, Pa
p_a	atmosphere pressure, Pa
Q_a	gas flowrate at P_a and slag temperature, m^3/s
r	slag splashing rate, kg/(m^3·s)
R	gas constant, 8.314 J/(mol·K)
R_ε	R-ε term, kg/(m·s^4)
R'	top radius of the slag pot, m
S	filtered rate of strain tensor, 1/s
t	time, s
T_{in}	temperature of the gas phase entering the slag pot, K
T_s	slag temperature, K
u	velocity, m/s
u_l	maximum linear velocity in the sloshing, m/s
v	component of the flow velocity parallel to the gravitational vector, m/s
V	total volume of the molten slag in the slag pot, m^3
w	component of the flow velocity perpendicular to the gravitational vector, m/s
z	axial distance from the bottom of slag pot, m

Greek symbols

α	phase volume fraction
$\alpha_k, \alpha_\varepsilon$	inverse effective Prandtl numbers
Δ	filtering width, m
ε	turbulent kinetic energy dissipation rate, m^2/s^3
η_{max}	maximum wave amplitude, m
η_1, η_2	energy conversion efficiencies
λ_2	second largest eigenvalue of a velocity gradient tensor
μ_{eff}	effective viscosity, Pa·s
μ_t	turbulent viscosity, Pa·s
ρ	density, kg/m^3
σ	surface tension coefficient
$\bar{\tau}$	stress tensor, N/m^2
ω	angular frequency, rad/s

Subscripts

g	gas phase
i,j	coordinate direction indices
l	liquid phase
q	qth phase

in a cylindrical bath. An empirical equation was derived to predict the gas penetration depth. The experimental results also confirmed the presence of a dead zone by measuring the mass transfer coefficient between a platinum plate and aqueous $FeSO_4$ solution. Mazumdar and Guthrie (1985) developed a computational scheme to predict the flow generated by both the partially and fully submerged gas injection in a steelmaking ladle. The accuracy of their calculation was evaluated by using a 0.3 scaled-down water modelling experiment. An agreement was achieved between the experimentally measured and mathematically predicted flow fields. Although a 2D simulation, their work has provided a basis of describing two-phase flow. Liovic et al. (2002) developed a 2D axisymmetric model with volume tracking technique to study the top submerged gas injection in a smelting process. It was concluded that a high liquid viscosity suppresses splashing and free surface distortion and reduces liquid backflow into the lance by calculating the distributions of gas and liquid phase in the gas-water/95% glycerol solution systems. Based on the recorded pressure in the lance and its Fourier transform, a bubbling frequency of 5 Hz was determined, which agrees with the value recorded in industrial smelters. Huda et al. (2010) investigated the characteristics of the top gas injection in a water bath by coupling the Euler-Euler model with the standard k-ε turbulence model. The simulated velocity field agrees well with the water model experiment (Morsi et al., 2000). A semi-empirical equation was proposed to calculate the penetration depth of the annulus air jet into the water bath. It was found that the mixing in the water bath predominately takes place near the lance and a recirculation zone is favorable for uniform mixing. However, a discrepancy of the mean tangential velocity was found between the simulation and the water model experiment, and it was considered to be caused by the poor performance of the standard k-ε model. A quantitative understanding of splashing cannot be achieved due to the absence of surface tracking methods. Later on, the same group applied this Euler-Euler-standard k-ε model in a zinc slag fuming process (Huda et al., 2012). The simulation predicted that the rate-limiting steps of Zn fuming are both the mass transfer of ZnO from the bulk slag to slag-gas interface and the gas-carbon reaction rate. Increasing the submerged lance depth could increase the fuming rate. In order to compare the calculation results of using different turbulence model on a top submerged gas injection into a high viscosity liquid, the present authors (Wang et al., 2018) performed 2D and 3D simulations with a combined VOF-RNG/RSM/LES model. The simulation was elaborately validated by PIV experiments in an air-paraffin oil two-phase system. The averaged feature of the flow generated by the top gas injection is captured by all of the three turbulence models, however, only the LES model can give a reasonable prediction of the generated turbulence. Bubble shape and rising behavior are well predicted by the 3D simulation in the study, where only a shallow lance submersion (l/L = 0.26) was used. This limits the reliability of the combined numerical model, because the submerged lance depth plays a significant role in the flow

Please cite this article as: Y. Wang, L. Cao, M. Vanierschot et al., Modelling of gas injection into a viscous liquid through a top-submerged lance, Chemical Engineering Science, https://doi.org/10.1016/j.ces.2019.115359

characteristics (Morsi et al., 2000; Huda et al., 2010). Obiso et al. (2019) studied the effect of liquid properties on the hydrodynamics of a smelting process by using the coupled Level Set-VOF model. The results highlighted the importance of the viscous and interfacial forces on gas injection in smelting slags. It was indicated that the Froude number is insufficient to characterize the flow. Only normalized numerical data were presented in their work, making it difficult to compare with other studies.

Based on the above literature study, it can be concluded that (1) compared to low viscosity liquids (such as water, mercury and Wood's metal), viscous liquids have been much less employed in physical modelling (Pan and Langberg, 2010; Huda et al., 2012; Wang et al., 2018; Sattar et al., 2014; Obiso et al., 2019); (2) the standard k-ε turbulence model is normally applied to the simulations, and a full validation of different turbulence model is necessary for the case with a large lance submerged depth; (3) the flow characteristics of a top gas injection in metallurgical processes have not been comprehensively investigated yet under industrially relevant conditions, for which simply the phenomenal descriptions of surface sloshing and splashing are available in literature, and a quantitative prediction of the phenomena is needed for process optimization.

In this context, a sharp surface tracking technique, VOF, is adopted in this paper to study the splashing and sloshing phenomena in the slag stabilization process. The RNG k-ε model is used in this work for the following reasons: (1) the choice of turbulence model is critical for simulation of the particle migration and mixing phenomena (Crowe et al., 1996; Jha et al., 2003); (2) the RNG k-ε model outperformed the standard k-ε model in rotating flows (Schwarze et al., 2001; Hou and Zou, 2005). In addition, the LES model, as an advanced turbulence model, is also applied for modeling the turbulence. Prior to the real case study, validations of the numerical model are performed for a large submerged lance depth case (l/L = 0.52). The numerical results are corroborated by PIV experiments of a paraffin oil-air system in a scale-down vessel at room temperature. In this way, the gas-liquid slag hydrodynamics of the slag stabilization process is systematically investigated with respect to the velocity attenuation, gas penetration depth, flow regime, surface sloshing, splashing and coherent structures identification. The purpose of this work is to develop a 3D numerical model with a coupling of the VOF and the RNG k-ε model or LES model for understanding the hydrodynamics in the slag stabilization process, such as the mixing characteristics of additives during the process. This work can also shed light on common features of a gas injection into a highly viscous liquid which is commonly present in chemical engineering process.

2. Numerical and experimental methodology

2.1. VOF model

In the VOF model, the phase volume fraction, α, is introduced to track the interface position. The tracking of the interface between phases throughout the domain is accompanied by solving a continuity equation for the volume fraction of the qth phase, as shown in Eq. (1). The volume fraction of the primary phase is computed by the constraint given in Eq. (2). In this calculation, an explicit formulation, *i.e.*, geometric reconstruction scheme developed by Youngs (Youngs, 1982), is adopted. It assumes that the interface has a linear slope within each cell, and this linear slope is used to calculate the face fluxes. The volume fraction in each cell is obtained based on the consequent face fluxes. This scheme has been considered as the most accurate one as a result of its small numerical diffusion (Yang et al., 2017;). In the VOF model variables are shared by all phases, therefore, only one set of momentum equations is solved in Eq. (3).

$$\frac{\partial}{\partial t}\left(\alpha_q \rho_q\right) + \nabla \cdot \left(\alpha_q \rho_q \vec{u}\right) = 0 \tag{1}$$

$$\sum_{q=1}^{n} \alpha_q = 1 \tag{2}$$

$$\frac{\partial}{\partial t}\left(\rho \vec{u}\right) + \nabla \cdot \left(\rho \vec{u}\,\vec{u}\right) = -\nabla p + \nabla \cdot \bar{\tau} + \rho \vec{g} + \vec{F}_{csf} \tag{3}$$

Since the bubble behavior and the liquid surface distortion are affected by the surface tension of the liquid, the surface tension force, a source term in the momentum conservation equation, is simulated based on the Continuum Surface Force (CSF) model developed by Brackbill et al. (1992). The surface tension force is expressed by:

$$\vec{F}_{csf} = \sigma K \nabla \alpha \tag{4}$$

2.2. Turbulence models

2.2.1. RNG model

The RNG model is developed by the Renormalization Group theory (Yakhot and Orszag, 1986). Like the widely used standard k-ε model (Launder and Spalding, 1974), it also requires two partial differential transport equations for the turbulent kinetic energy, k, and its dissipation rate, ε. The form of the transport equations is similar to that of the standard k-ε model. However, necessary modifications are made in the RNG model to increase its accuracy for the rapidly strained flows and swirling flows. The transport equations are shown as Eqs. (5) and (6). After solving these two equations, the eddy viscosity is computed and then the Reynolds stress terms are obtained closing the Reynolds Averaged Navier-Stokes (RANS) equations.

$$\frac{\partial}{\partial t}(\rho k) + \frac{\partial}{\partial x_i}(\rho k u_i) = \frac{\partial}{\partial x_j}\left(\alpha_k \mu_{eff} \frac{\partial k}{\partial x_j}\right) + G_k + G_b - \rho\varepsilon \tag{5}$$

Table 1
Geometrical dimensions, operational parameters and material properties used in physical modelling and slag stabilization process.

Physical modelling	
Dimensions (X × Y × Z), m	0.135 × 0.135 × 0.195
Inner diameter of lance, m	0.005
Outer diameter of lance, m	0.008
Height of paraffin oil level, m	0.168
Lance submergence depth, m	0.088
Air flow rate, Nm^3/h	0.5
Pressure, kPa	120
Density of paraffin oil, kg/m^3	880
Viscosity of paraffin oil, $kg{\cdot}m^{-1}{\cdot}s^{-1}$	0.065
Density of air, kg/m^3	1.225
Viscosity of air, $kg{\cdot}m^{-1}{\cdot}s^{-1}$	1.789×10^{-5}
Interfacial tension of oil/air, N/m	0.026
Industrial slag stabilization process	
Top diameter of the slag pot, m	3.36
Bottom diameter of the slag pot, m	2.39
Height of the slag pot, m	3.558
Lance diameter of the slag pot, m	0.04
Height of slag level, m	3.0
Lance submergence depth (slag pot), m	0.3, 0.65, 1.0
Gas flow rate, Nm^3/h	40–200
Pressure, kPa	300
Density of slag, kg/m^3	3000
Viscosity of slag, $kg{\cdot}m^{-1}{\cdot}s^{-1}$	0.1
Density of gas, kg/m^3	0.574◆
Viscosity of gas, $kg{\cdot}m^{-1}{\cdot}s^{-1}$	5.87×10^{-5} *
Interfacial tension of slag/gas, N/m	0.55

"◆" and "*" indicate calculated values based on the ideal gas law and Sutherland's law (Sutherland, 1893), respectively.

Please cite this article as: Y. Wang, L. Cao, M. Vanierschot et al., Modelling of gas injection into a viscous liquid through a top-submerged lance, Chemical Engineering Science, https://doi.org/10.1016/j.ces.2019.115359

$$\frac{\partial}{\partial t}(\rho\varepsilon)+\frac{\partial}{\partial x_i}(\rho\varepsilon u_i)=\frac{\partial}{\partial x_j}\left(\alpha_\varepsilon\mu_{eff}\frac{\partial\varepsilon}{\partial x_j}\right)+C_{1\varepsilon}\frac{\varepsilon}{k}(G_k+C_{3\varepsilon}G_b)-C_{2\varepsilon}\rho\frac{\varepsilon^2}{k}-R_\varepsilon \quad (6)$$

$$C_{3\varepsilon}=\tanh\left|\frac{v}{w}\right| \quad (7)$$

2.2.2. LES model

Due to the presence of multi-scale turbulence in the multiphase flow in this work, an advanced turbulence model, the LES model, is employed. Unlike the commonly used k-ε model, the instantaneous Navier-Stokes (N-S) equations are subjected to a filtered operation instead of a Reynolds averaging method, resulting in grid scale and subgrid scale (SGS) components. The grid scale component is resolved directly, and the SGS component is modelled by the established SGS model. In this study, two built-in SGS models are used, *i.e.*, the Dynamic Smagorinsky-Lilly (DSL) model and the Wall-Adapting Local Eddy-Viscosity (WALE) model.

Smagorinsky (Smagorinsky, 1963) proposed a model to compute the eddy viscosity, as shown in Eq. (8). To optimize the model, it is needed to carefully choose the model constant, C_s, which can be dynamically calculated through a procedure developed by Germano et al. (1991) and Lilly (1992). In the dynamic procedure, a second filter called test filter, in which the width is twice as large as that of the original filter, is applied to filter the N-S equations, resulting in a second resolved field. The information obtained from the scale size between the original filter and the test filter is used to calculate the C_s. In addition to the DSL model, the WALE model (Nicoud and Ducros, 1999) is adopted to model the SGS turbulence. Since this model can correctly evaluate the laminar zone in the calculation domain, it is appropriate for our case, where a complete turbulent flow will be expected in the middle of the domain and a laminar flow near the wall due to a high liquid viscosity.

$$\mu_t=\rho(C_s\Delta)^2\left|\bar{S}\right| \quad (8)$$

2.3. Numerical setup

The simulations are performed using the commercial software package ANSYS FLUENT 16.2. The geometrical information, operational parameters and materials properties used in the physical modelling and the industrial slag stabilization process are listed in Table 1. Geometries of the physical model and the industrial slag pot are depicted in Fig. 1. The whole domain is patched by two zones, *i.e.*, the gas zone and the liquid zone. The boundary between the two zones is set as interface. The remaining boundary conditions, *i.e.*, velocity inlet, pressure outlet and wall, are also

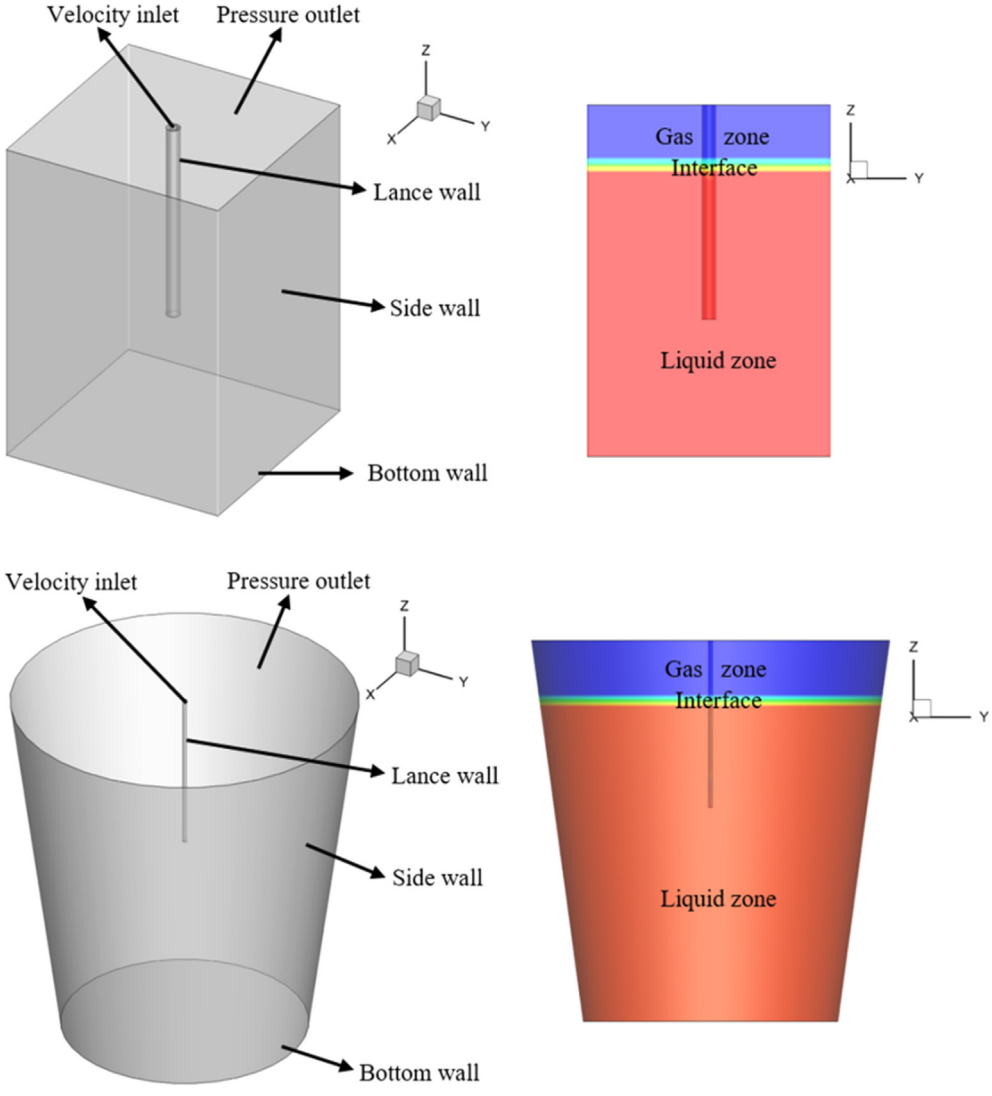

Fig. 1. Geometry and boundary conditions of the physical model (upper) and the slag pot (lower).

Please cite this article as: Y. Wang, L. Cao, M. Vanierschot et al., Modelling of gas injection into a viscous liquid through a top-submerged lance, Chemical Engineering Science, https://doi.org/10.1016/j.ces.2019.115359

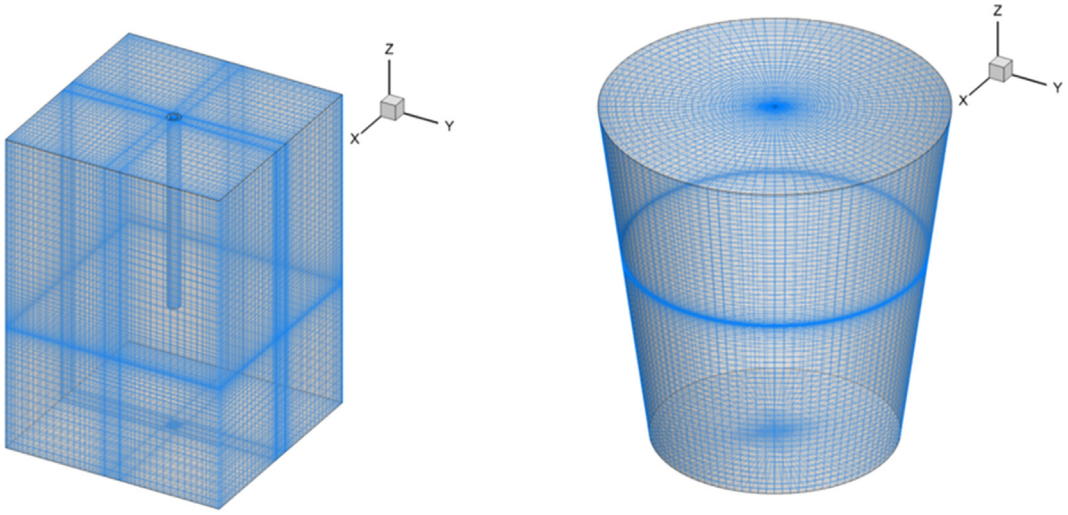

Fig. 2. Meshes of the physical model (left) and the slag pot (right).

indicated in Fig. 1. The structured meshes are established with the ICEM software. According to the grid independency study in our previous work (Wang et al., 2018), a mesh with 355,603 hexahedral cells is sufficient for the simulation of the physical model. The grid size ranges from 0.3 mm to 4.0 mm. For the slag pot, two meshes with number of hexahedral cells of 481,440 and 578,880 are used to perform a mesh independency study before the simulation of flow characteristics. The grid size ranges from 1 mm to 123 mm for the mesh of 481,440 cells and ranges from 0.83 mm to 104 mm for the other mesh. Taken into account a large velocity gradient in the lance region, the mesh is refined in the region. The mesh with coarse grids is generated in the near-wall region to save the computational cost, since the near-wall region is not of interest in the work. The law-of-the-wall algorithm is employed as the near-wall treatment method. The representative meshes are given in Fig. 2.

The Semi-Implicit Method for Pressure-Linked Equations – Consistent (SIMPLEC) scheme (Van Doormaal and Raithby, 1984) is adopted for the solution of the velocity-pressure coupling equation. The spatial discretization schemes for the pressure and momentum equations are PREssure STaggering Option (PRESTO!) and bounded central differencing, respectively. Convergence is determined by monitoring the unscaled residual of the continuity equation. In this study, it is considered that a sufficient accuracy is achieved when the residual of the continuity equation drops at least 3 orders of magnitude. The convergence criterion is set as 1×10^{-7}. In order to capture the detailed temporal features of the flow, the time step should be smaller than the minimum system time scale which is approximately 1.04×10^{-5} s. Therefore, the time step of 1×10^{-5} s is adopted by considering both the simulation accuracy and the computational cost, resulting in a global Courant number of 0.65. Part of the calculations were submitted to a High Performance Computing cluster and one node with 20 processors was required. The rest were performed in a group workstation (Intel(R) Xeon(R) Gold 5120 CPU@2.20 GHz with 16 cores). It took around five months to finish all the calculations.

2.4. Experimental method

Paraffin oil and compressed air are used to form a two-phase flow. The PIV experiment setup is given in Fig. 3. In order to make the experiment dynamically similar to the industrial slag stabilization process, the modified Froude number, defined as the ratio of the inertial force to the buoyancy force in Eq. (9), is adopted to determine the top gas flow rate (Singh et al., 2007). The submerged lance depth is chosen as the characteristic length for the calculation of the modified Froude number. The modified Froude number in the physical modelling is approximately 0.06, which is within the range of the modified Froude number (*i.e.*, 0.008–0.18) in the slag stabilization process. This enables the physical modelling to reflect well the flow characteristics in the slag pot. It is worth mentioning that the gas-liquid interfacial tension in the two systems is different. The interfacial phenomena such as bubble breakup and coalescence, which are greatly affected by the interfacial force, may not be realistically represented. However, such interfacial phenomena are not the main interests and excluded in this work. Future work is needed for resolving detailed interfacial phenomena. The flow information is measured by the Particle Imaging Velocimetry (PIV) technique. In order to explain the obtained velocity profile in the following section, the measured zone in PIV experiment is shown in Fig. 3. Considering the maximal pixel

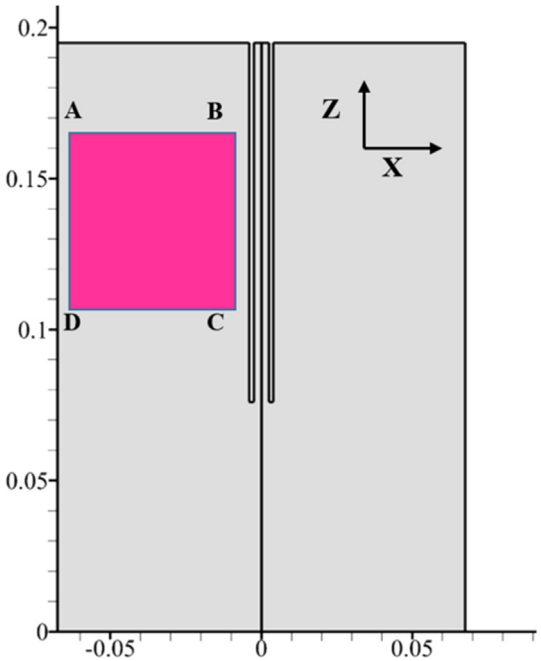

Fig. 3. PIV measured zone (red area 0.058 m × 0.058 m): A (−0.065 m, 0.164 m); B (−0.007 m, 0.164 m); C (−0.007 m, 0.106 m); D (−0.065 m, 0.106 m). (For interpretation of the references to colour in this figure legend, the reader is referred to the web version of this article.)

Please cite this article as: Y. Wang, L. Cao, M. Vanierschot et al., Modelling of gas injection into a viscous liquid through a top-submerged lance, Chemical Engineering Science, https://doi.org/10.1016/j.ces.2019.115359

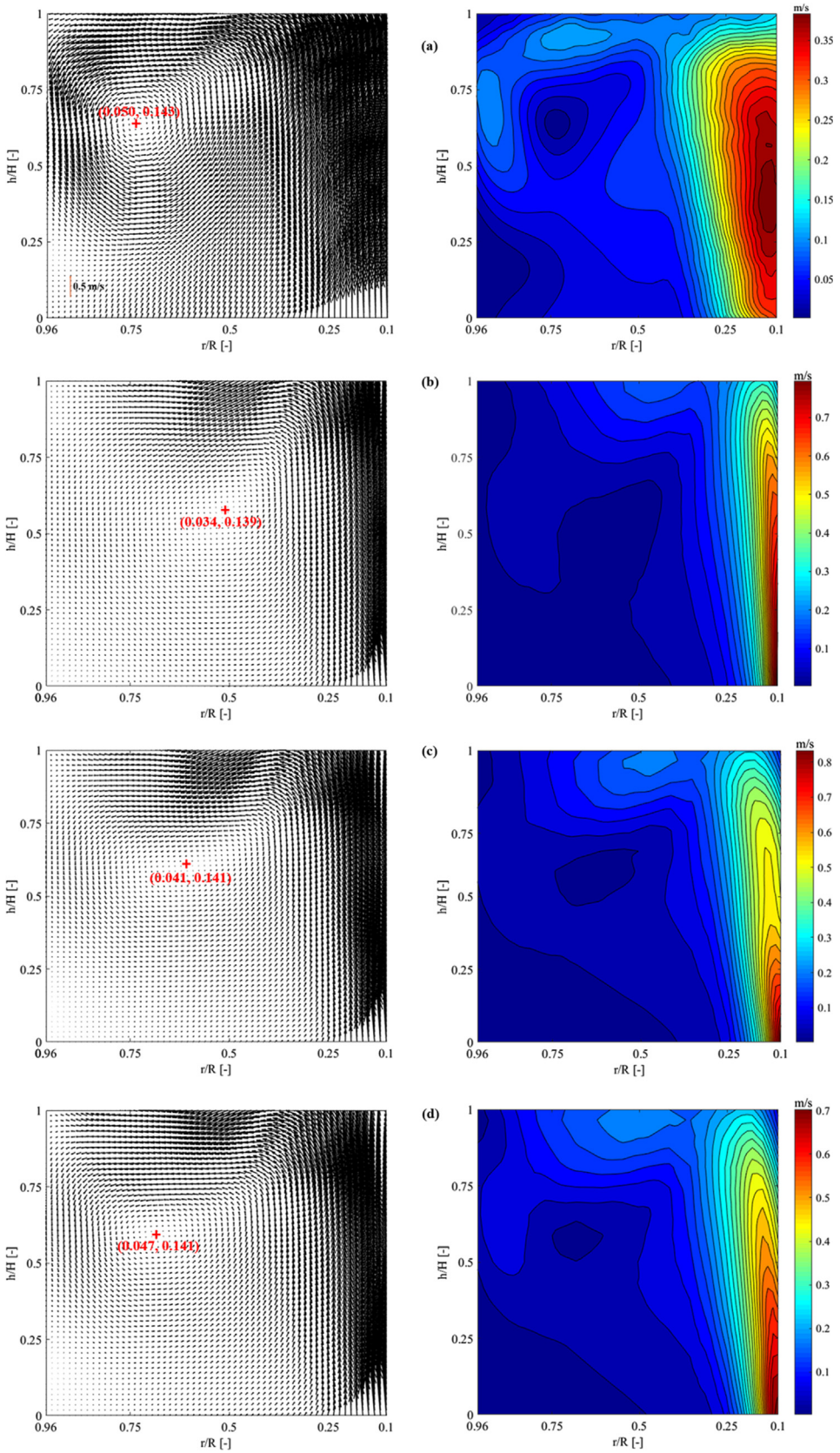

Fig. 4. Experimentally measured and numerically modelled velocity fields (a) Experimental; (b) RNG model; (c) LES-WALE model; (d) LES-DSL model (r: radial distance from the axial line; R: radial distance between the axial line and the vessel wall; h: axial distance from the bottom of the measured zone; H: height of the measured zone).

Please cite this article as: Y. Wang, L. Cao, M. Vanierschot et al., Modelling of gas injection into a viscous liquid through a top-submerged lance, Chemical Engineering Science, https://doi.org/10.1016/j.ces.2019.115359

displacement, the relative error of the instantaneous velocity vectors of the PIV experiments is maximal 2%. The sampling error on the mean velocity is estimated based on the sampling size of 1024 and was estimated to be less than 2%. Therefore, the total relative error is around 3%. The detailed procedure and conditions of the PIV measurement can be found in the work of Wang et al. (2018) and Vanierschot et al. (2014).

$$Fr_m = \frac{\rho_g {u_g}^2}{\left(\rho_l - \rho_g\right) g H_c} \tag{9}$$

3. Results and discussion

3.1. Experimental validation

3.1.1. Qualitative validation

Velocity vector and velocity contour profiles obtained from the PIV experiment and simulation are represented in Fig. 4. Apparently, a counter-clockwise rotating vortex in the investigated zone is visualized both in experiment and simulation. The vortex core is indicated by a red cross mark in the velocity vector, and its X and Z

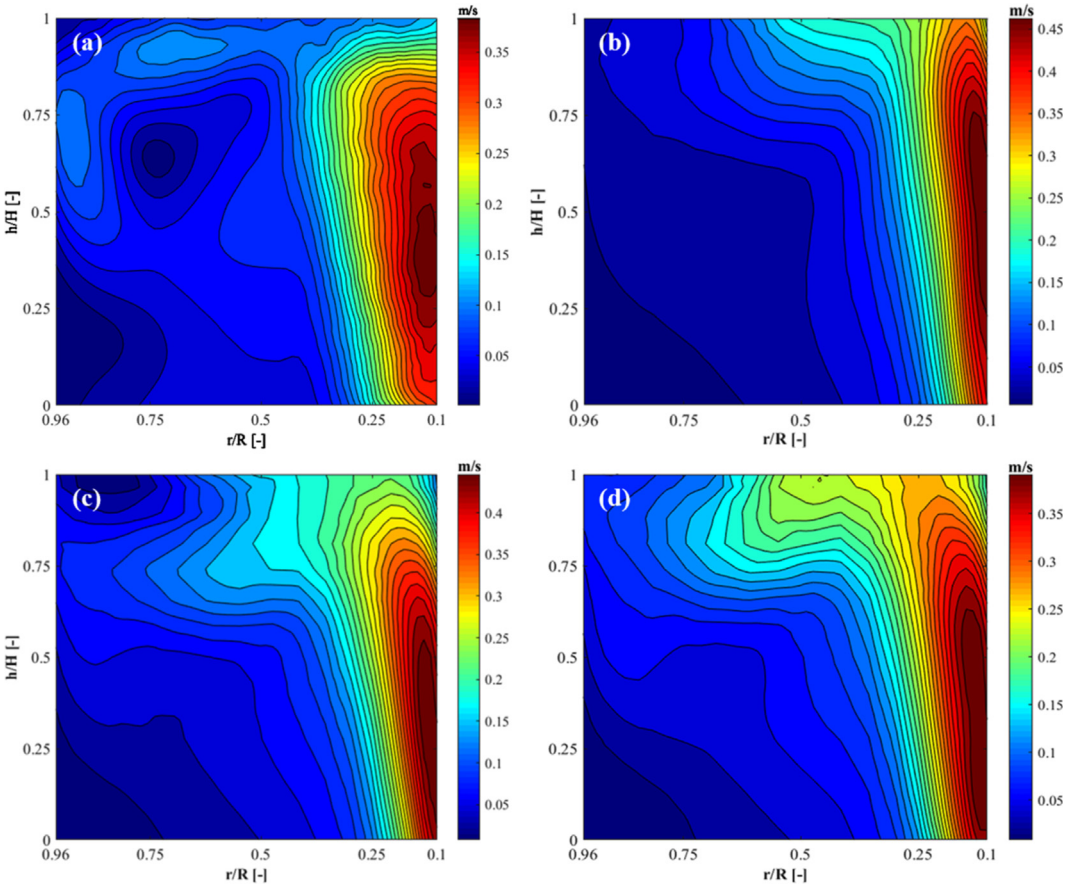

Fig. 5. Liquid velocity contour profile from (a) Experiment; (b) RNG model; (c) LES-WALE model; (d) LES-DSL model (r: radial distance from the axial line; R: radial distance between the axial line and the vessel wall; h: axial distance from the bottom of the measured zone; H: height of the measured zone).

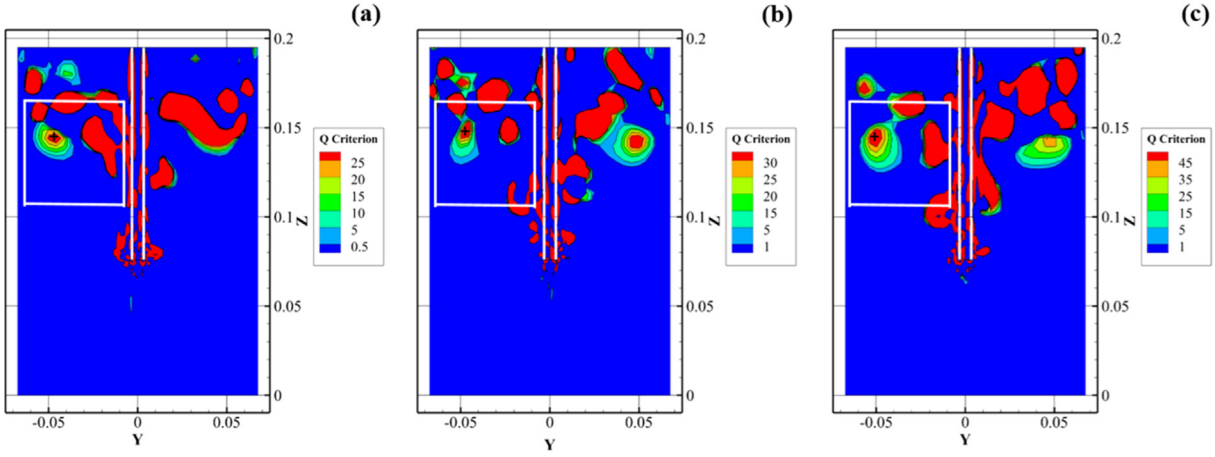

Fig. 6. Vortex profiles of VOF-LES-WALE model at different instants in X-Z plane (a) 3.5 s; (b) 5 s; (c) 10 s.

Please cite this article as: Y. Wang, L. Cao, M. Vanierschot et al., Modelling of gas injection into a viscous liquid through a top-submerged lance, Chemical Engineering Science, https://doi.org/10.1016/j.ces.2019.115359

coordinates are given in the figure. By comparing the coordinates, it was found the VOF-LES-DSL model surpasses the VOF-RNG and VOF-LES-WALE models in predicting this macroscopic recirculation. As another main feature of the flow, a large velocity gradient is observed in both experiment and simulation. Velocities with a range of 0.4–0.8 m/s are calculated in the area near the top lance as shown by the green-red transition zone in Fig. 4(b)–(d). However, velocities less than 0.15 m/s are observed in the region adjacent to the vessel wall at r/R = 1. Compared to the numerical results, a small velocity gradient is obtained in the experiment. This can be seen in the right part of Fig. 4(a), where the maximum measured velocity is less than 0.4 m/s. The discrepancy of the velocity magnitude in the near-lance region between the experiment and simulation could be caused by the presence of gas bubbles. Due to the refractive issue of the gas bubble, the measured value is negatively influenced. Apart from that, the velocity obtained from the simulation is a volume-averaged value of both gas and liquid phase, instead of the pure liquid velocity as measured in the PIV experiment. Since the gas velocity is much larger than the liquid velocity, the volume-averaged velocity in the simulation is significantly overestimated in the high void fraction region. To obtain an averaged velocity of the liquid phase for a further model validation, the gas velocity is filtered out of the final averaged velocity by adopting the post-processing method proposed by Obiso et al. (2019). The liquid velocity contour profiles are shown in Fig. 5, where the velocity magnitudes are greatly decreased, namely, from 0.74 m/s to 0.46 m/s in the RNG model, from 0.81 m/s to 0.44 m/s in the LES-WALE model and from 0.7 m/s to 0.39 m/s in the LES-DSL model. The obtained maximum liquid velocity, especially the value from the LES-DSL model, is very close to the experimental result which is around 0.38 m/s. Therefore, it is reasonable to conclude that the findings confirm the explanation for the velocity deviation in the near-lance region. The average velocity mentioned in the following is the volume-averaged velocity unless indicated explicitly.

3.1.2. Quantitative validation

For a quantitative validation, data along a line through the vortex core are extracted and compared with the measured value. The vortex core is identified. In this study, the Q-criterion (Hunt et al., 1988) based on the positive second invariant, Q, of the velocity gradient tensor is adopted for the identification of the vortex core. The instantaneous Q values of the VOF-LES-WALE model are shown as an example in Fig. 6. The white square indicates the measured zone, and the black cross marks the vortex core. It should be noted that only the vortex core in the measured zone is of our interest. Except in the lance area, the vortex in the measured zone is similar with each other at three different moments (see Fig. 6(a)–(c)), suggesting a steady flow in this region. The instantaneous structure with a larger Q value in the lance area and top gas zone is induced by the rising gas and it varies with time. The position of the vortex core changes slightly (see Fig. 6) and agrees with that of the vortex core in the left part of Fig. 4(c). Based on this, data along the horizontal line h = 0.141 m are extracted for the case VOF-LES-WALE. The same treatment is repeated, and the data along the horizontal lines h = 0.139 m and h = 0.141 m are extracted for the cases VOF-RNG and VOF-LES-DSL, respectively.

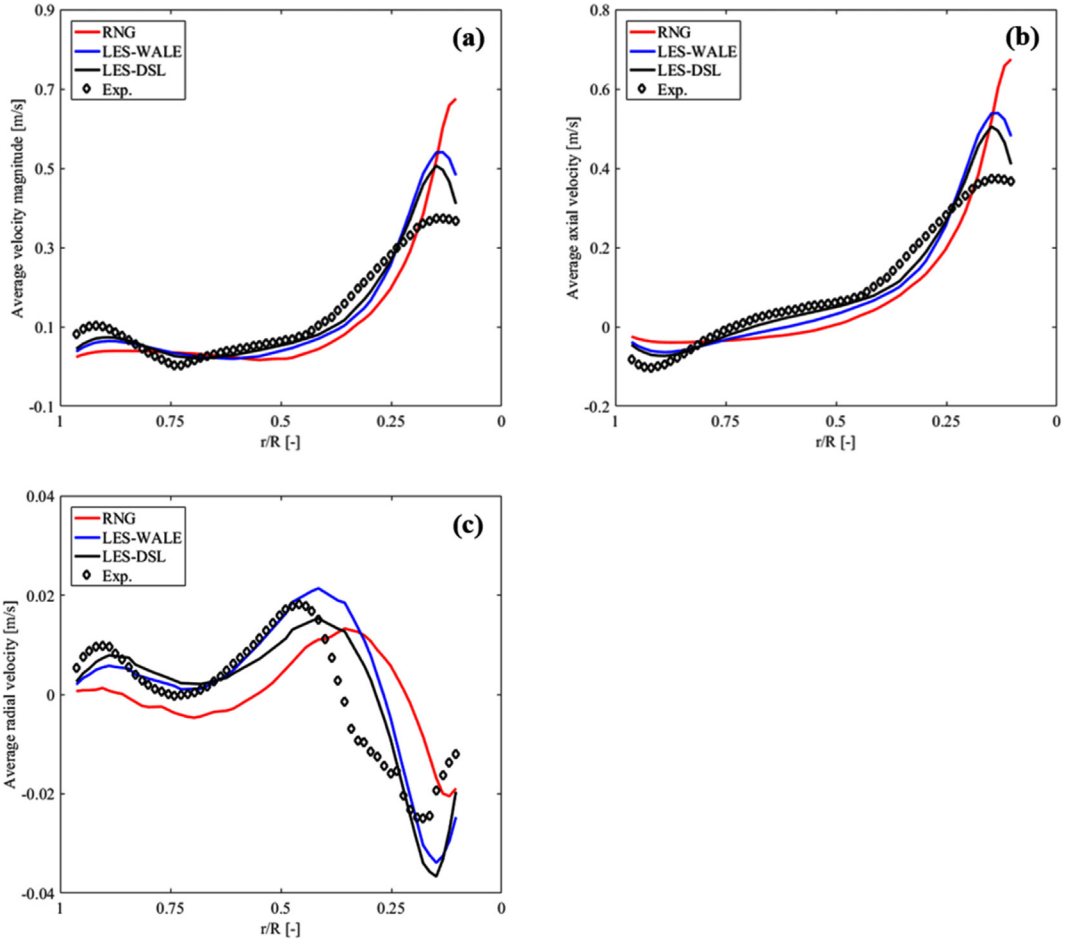

Fig. 7. (a) Average velocity magnitude; (b) Average axial velocity; (c) Average radial velocity along the line through the vortex core.

Please cite this article as: Y. Wang, L. Cao, M. Vanierschot et al., Modelling of gas injection into a viscous liquid through a top-submerged lance, Chemical Engineering Science, https://doi.org/10.1016/j.ces.2019.115359

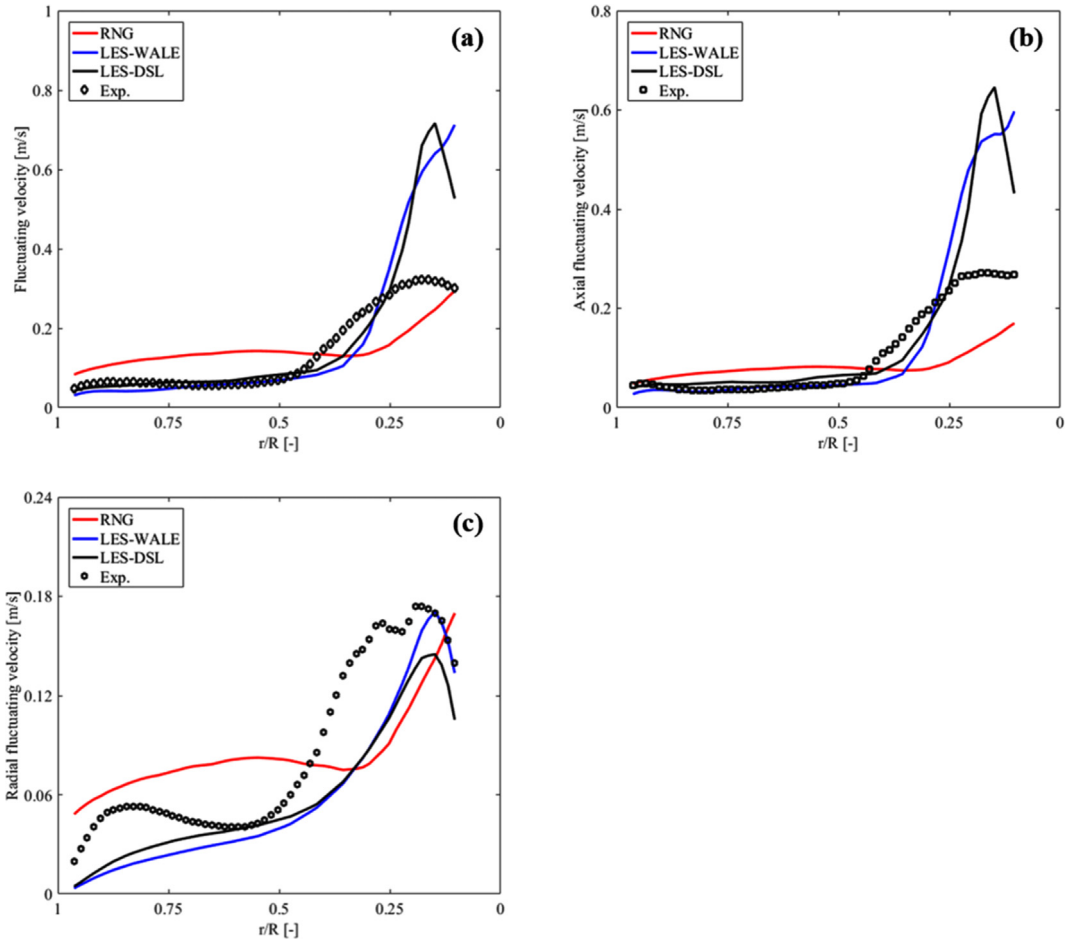

Fig. 8. (a) Velocity fluctuation; (b) Axial velocity fluctuation; (c) Radial velocity fluctuation along the line through the vortex core.

The time-averaged velocity magnitude and its two components, namely, axial velocity magnitude (z direction) and radial velocity magnitude (x direction) are plotted in Fig. 7. In general, the measured result agrees well with simulation (VOF-RNG/LES), except in the region near the top lance (r/R = 0). The maximum deviation is approximately 84%, 44% and 36%, respectively, for the RNG, LES-WALE and LES-DSL simulation. The reason has been explained in section 3.1.1. It can be concluded that the simulations in this study have captured the averaged features of the top injection flow. The LES model performs better than the RNG model in predicting the velocities. This might be due to the different treatment of the instantaneous N-S equations, namely, Reynolds-averaging algorithm for the RNG model and the filtering algorithm for the LES model. In the RNG simulation, the Reynolds-averaging velocity is directly obtained, while the velocity fluctuation is included in the turbulent kinetic energy. However, the instantaneous velocity of the large eddy is obtained in the LES model, and then averaged to obtain a mean value. Since the mesh grid is dense enough, it is considered that the mean velocity value from the LES model can represent the reality. The result of the DSL model slightly outperforms that of the WALE model with respect to the average velocity and its axial component. These two SGS models give a comparable result with each other in the radial velocity. The DSL model is superior in the shear region (r/R < 0.4) close to the top lance, but the WALE model performs better in the less sheared region (r/R > 0.5). Compared to the axial velocity, the radial velocity is more difficult to be predicted as the buoyancy-driven flow is dominated in the axial direction. Overall, the DSL model performs slightly better than the WALE model in this work.

Fig. 8 shows the velocity fluctuations which are obtained by calculating the root-mean-square (RMS) values of the instantaneous velocities. There is a clear discrepancy between the RNG results and the experimental data. The failure of the RNG model might be attributed to the use of the turbulence dissipation rate equation in the model. The inaccurate prediction of the turbulence

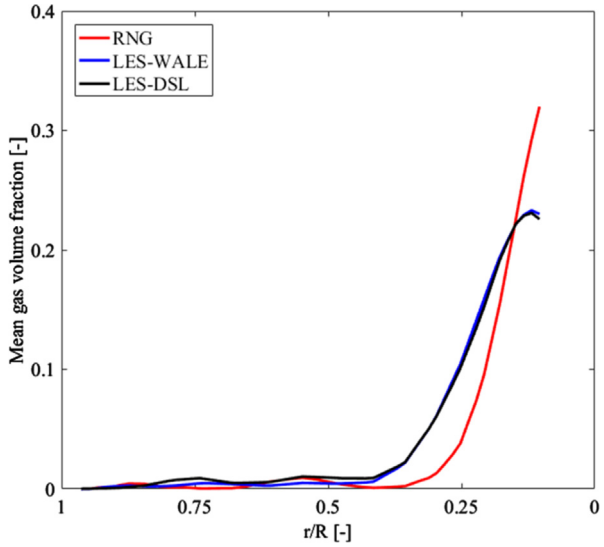

Fig. 9. Mean gas volume fraction along the line through the vortex core.

Please cite this article as: Y. Wang, L. Cao, M. Vanierschot et al., Modelling of gas injection into a viscous liquid through a top-submerged lance, Chemical Engineering Science, https://doi.org/10.1016/j.ces.2019.115359

dissipation rate decreases the precision degree of the RNG model. Compared to the RNG model, the LES model predicts the velocity fluctuation well and its axial component in the region of r/R > 0.25, and over-estimates the fluctuations in the region where gas bubbles are concentrated (r/R < 0.25). Fig. 9 shows that the gas volume fraction sharply increases in the region of r/R < 0.25, indicating the presence of gas phase in that region. A possible explanation for the disagreement can be an underestimation of the turbulent viscosity, which makes the induced turbulence less dissipated. In the LES-WALE model, the model constant C_w is grid-dependent and fixed *a priori* (Nicoud and Ducros, 1999). The C_w value used in the simulation may be smaller than the actual value in the bubbly region. As a consequence, the turbulent viscosity can be underestimated. Unlike the WALE model, the DSL model dynamically calculates the model constant, C_s, obtaining the turbulent viscosity based on the calculated model constant. The DSL model exhibits a slight advantage over the WALE model in predicting the velocity fluctuation. Like the average radial velocity, the radial velocity fluctuation is not as well evaluated as the axial velocity fluctuation. Nonetheless, a similar radial velocity fluctuation profile with two humps is observed between the WALE/DSL model and experiment.

3.1.3. 2D versus 3D simulations

In our previous study (l/L = 0.26) (Wang et al., 2018), only minor difference of the average axial velocity was observed between 2D and 3D VOF-LES-WALE simulations. This agrees with the findings of Lakehal et al. (2002), where the LES-SL/DSL models were adopted. However, in their study the 2D simulation obtained a better result than the 3D simulation in predicting the velocity fluctuation. Apparently this is not reasonable because the LES model is conceptually three dimensional. In order to clarify this point, the average velocity and velocity fluctuation obtained from the RNG/LES-DSL/WALE models are respectively compared in Figs. 10 and 11 for l/L = 0.52. It is clear that the average flow velocity is well predicted by both 2D and 3D simulations, meaning that the flow is statistically two dimensional. However, difference of the velocity fluctuation is pronounced between 2D and 3D simulations. The 3D simulation obviously surpasses the 2D simulation for all of the three models. It is worth mentioning that the velocity fluctuation obtained in 2D simulation has a good agreement between the LES-WALE model and experiment (l/L = 0.26) (Wang et al., 2018). This may be due to the less vigorous fluctuation in the case with a small submerged lance depth. Apparently, a 3D simulation is necessary for vigorous fluctuation case.

3.2. Flow characteristics of the slag stabilization process

According to the experimental validation in Section 3.1, the combined VOF-LES-DSL model is adopted for the following parameter studies on the industrial slag stabilization process. Firstly, a mesh independency study is implemented and the results are shown in Fig. 12. The comparisons of the time-averaged velocity magnitudes extracted from z/L = 5/6 and z/L = 2/3 indicate no large deviation in most of the region. However, approximately 25% and 40% of deviations are observed in the near-lance region for z/

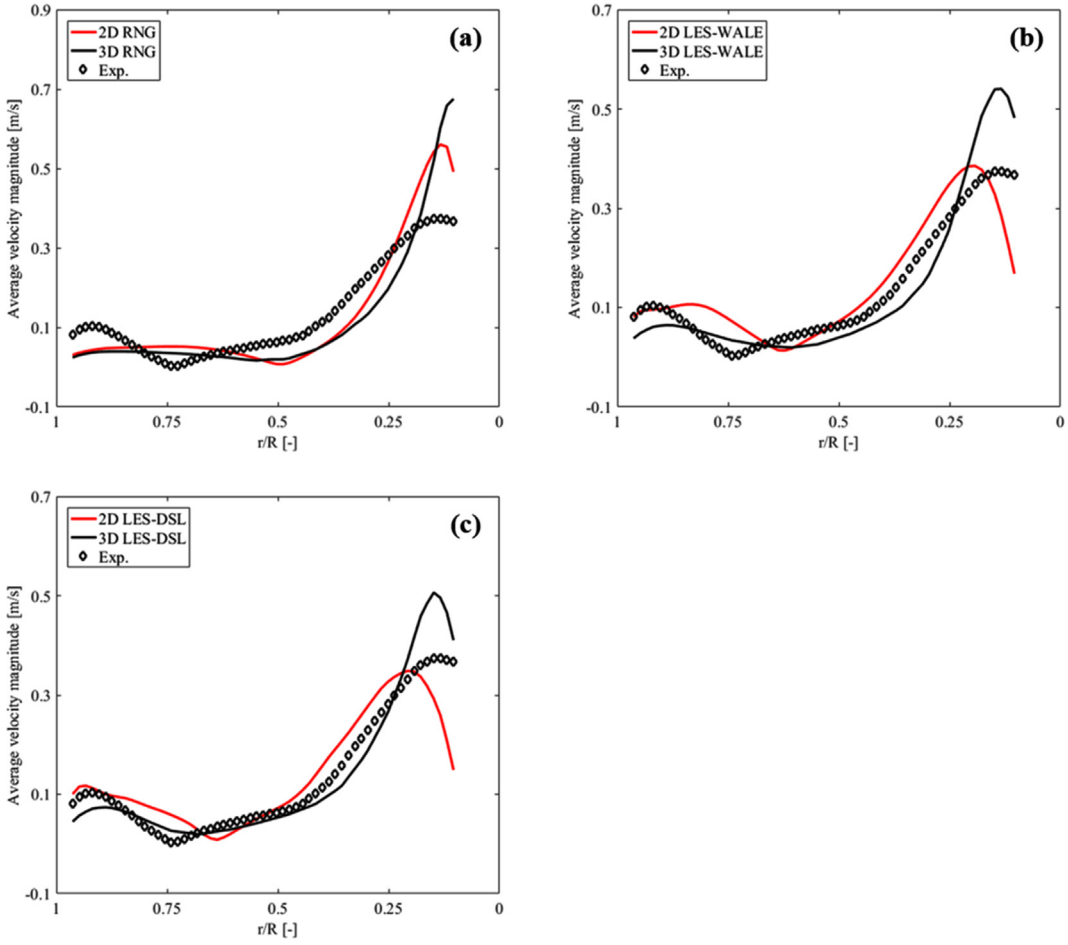

Fig. 10. Average velocity magnitudes along the line through the vortex core from 2D and 3D simulations (a) RNG; (b) LES-WALE; (c) LES-DSL.

Please cite this article as: Y. Wang, L. Cao, M. Vanierschot et al., Modelling of gas injection into a viscous liquid through a top-submerged lance, Chemical Engineering Science, https://doi.org/10.1016/j.ces.2019.115359

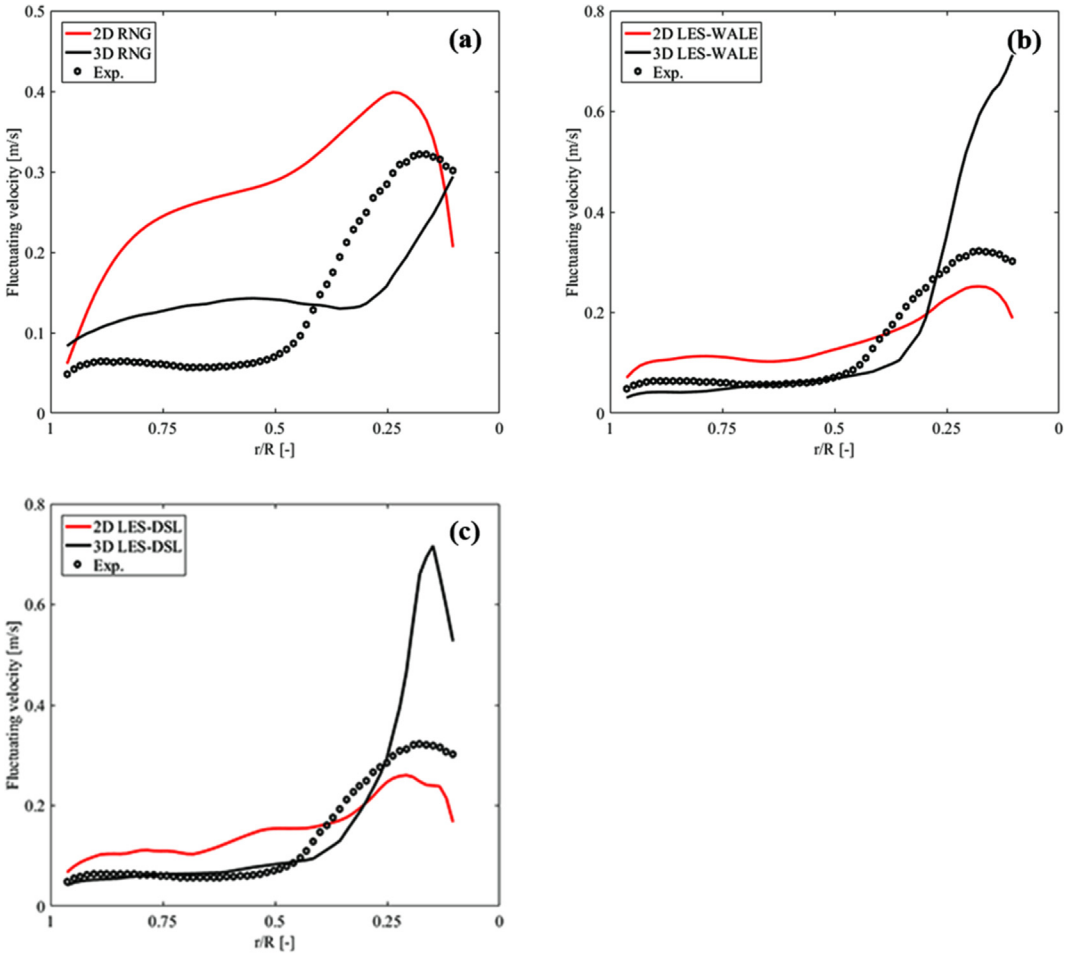

Fig. 11. Velocity fluctuations along the line through the vortex core from 2D and 3D simulations (a) RNG; (b) LES-WALE; (c) LES-DSL.

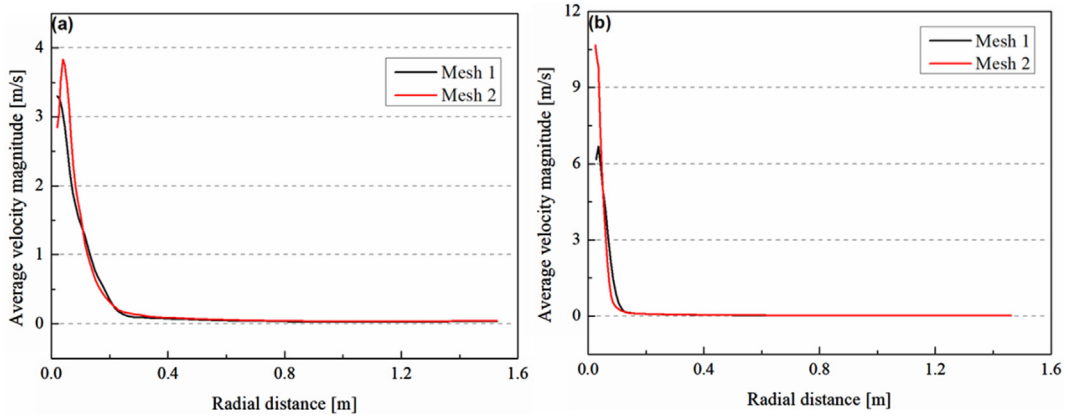

Fig. 12. Average velocity magnitude along (a) z/L = 5/6 and (b) z/L = 2/3 for different numbers of cells (Mesh 1: 481,440 cells; Mesh 2: 578,880 cells; z: axial distance from the bottom of slag pot; L: liquid level).

L = 5/6 and z/L = 2/3, respectively. The mesh density has direct influence on the calculation of the gas volume fraction, which affects the resulting velocity magnitude. This could be the reason for the deviation in the near-lance region where the gas bubbles are mainly concentrated. The purpose of our current work is to provide insights into the general flow characteristics of a top-submerged lance flow at industrially relevant conditions, but not to present all the detailed flow information. Hence, the mesh with 481,440 cells is selected for the following flow characteristics simulation by considering its accuracy and computational cost.

3.2.1. Gas penetration depth

The gas penetration depth, D_P, is a measure of the inertial momentum accompanied with the carrier gas into the molten slag. Larger momentum creates stronger agitation, resulting in a better mixing. The penetration depth in this work is defined as the distance from the lance exit to the axial position where α_g equals

Please cite this article as: Y. Wang, L. Cao, M. Vanierschot et al., Modelling of gas injection into a viscous liquid through a top-submerged lance, Chemical Engineering Science, https://doi.org/10.1016/j.ces.2019.115359

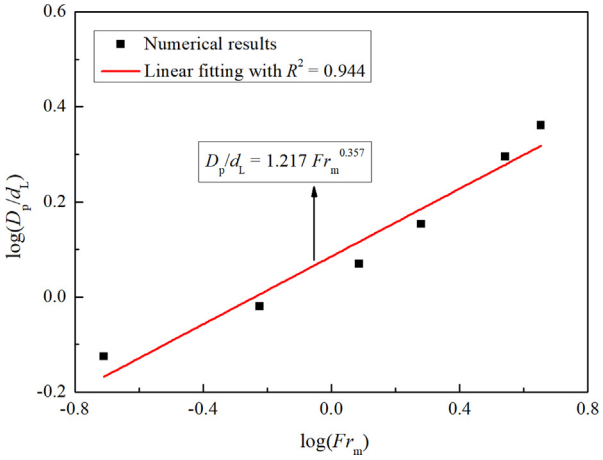

Fig. 13. Relationship between the penetration depth and the modified Froude number (l = 1.0 m).

0.5 on the centerline of the slag pot. According to previous studies (Iguchi et al., 1994; Huda et al., 2010); D_P is a function of Fr_m. In order to compare our results with those in the literature, the lance diameter d_L is used as the characteristic length in the Fr_m calculation. To correlate D_P with Fr_m, the simulation is carried out with six levels of the gas flow rate. As a result, a linear relationship of $\log\left(\frac{D_P}{d_L}\right)$ and $\log(Fr_m)$ is obtained as plotted in Fig. 13, and this semi-empirical equation is given in Eq. (10). This is quite similar with the experimentally measured result (see Eq. (11)) in different systems by Iguchi et al. (1994). The exponents in the two relations are very close, whereas the constant is different. This is considered to be caused by the distinct materials and vessel geometries applied in the respective studies.

$$D_P = 1.217 d_L Fr_m^{0.357} \tag{10}$$

$$D_P = 4.10 d_n Fr_m^{0.333} \tag{11}$$

3.2.2. Attenuation of flow velocity

Fig. 14 shows the attenuation of the mean velocity and turbulent kinetic energy as a function of the inlet gas velocity. After the injection the flow velocity decreases rapidly to almost zero within a very short distance, *i.e.* 0.15 m, for all of the inlet gas velocities in this work. This is due to a large density difference between the gas and molten slag phases. A large velocity gradient forms in the region near the lance tip, generating a strong shear-induced turbulence as well (seen Fig. 14(b)). At the distance larger than 0.15 m, the turbulent kinetic energy tends to be zero. This change tendency in turbulent kinetic energy is in line with that in average velocity (Fig. 14(a)). Taking the case with inlet velocity of 96.0 m/s as an example, the turbulent intensity and two derivatives, i.e., du_z/dy and du_z/dx at 10 s are depicted in Fig. 15(a)–(c), respectively. The turbulent intensity is very high in the lance tip region, and the shear stress represented by the two derivatives is large in this region. Therefore, the turbulence in this region is mainly induced by the shear stress. The latter results from the injected gas. Since an asymmetric phenomenon is also observed, asymmetric bubble behavior can be expected.

3.2.3. Flow regime

Understanding of the flow regime (namely, bubbling, jetting or transition) (Hoefele and Brimacombe, 1979; Zhao and Irons, 1990; Ruzicka et al., 1997) of gas injection into liquid slag through a top-submerged lance is of critical importance for the process optimization. In this work, pressure signals monitored at two positions with the coordinates of (0 m, 0 m, 2.5 m) and (0 m, 0 m, 3.0 m) in the lance (see Fig. 16) are averaged and then used to characterize the flow regime in the slag pot. In order to avoid the unstable flow at the initial stage, the pressure data were sampled after approximately 30 s. The sampling period lasts around 30 s. Since the flow becomes rather stable after 30 s, the sampled data show a similar change tendency. Only a part of the average pressure trace and its FFT results are shown in Fig. 17, where irregular and non-periodic pressure bursts are clearly observed. These bursts generate when the continuous gas jet is narrowed down or even necked off by the molten slag backflow from the adjacent region of the lance tip. The number of bursts decrease with increasing gas velocity (see Fig. 17(a) and (b)). This can be explained by the increased power (see Fig. 17(c) and (d)) of the injected gas, preventing slag backflow. Hence, the steady jetting behavior becomes more dominant at the larger inlet velocity. The FFT technique (Cooley et al., 1969; Brigham, 1988) is employed to further confirm this flow regime. Apparently, there is no dominant frequency in FFT patterns for both the cases, indicating no bubbling regime in the flow. There are peaks observed with different amplitudes, which is considered to be the noise generated by the system. Based on this analysis it can be concluded that under the given gas injection conditions the flow shows jetting behavior with a pulsing feature. In the slag stabilization treatment, however, fine solid additives are injected with the gas phase, and the apparent density of the mixture is much larger than that of the pure gas phase. This leads to an increase of gas-to-liquid density ratio, resulting in an enhancement of the jetting behavior and a deeper penetration depth (Zhao and Irons, 1990). This influences solid additive mixing. Although the effect of the coupling of the gas phase and solid additives is worthwhile to be investigated, it is not considered in this work.

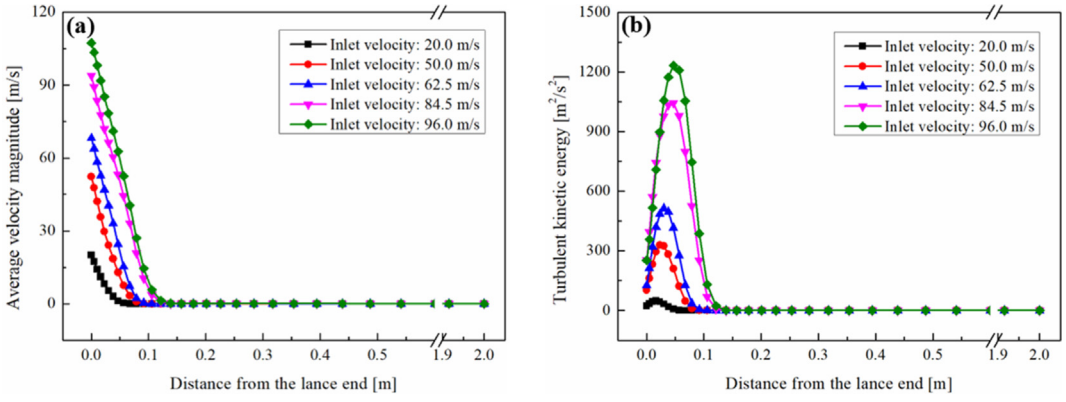

Fig. 14. (a) Average velocity and (b) Turbulent kinetic energy along the injected axis (l = 1.0 m).

Please cite this article as: Y. Wang, L. Cao, M. Vanierschot et al., Modelling of gas injection into a viscous liquid through a top-submerged lance, Chemical Engineering Science, https://doi.org/10.1016/j.ces.2019.115359

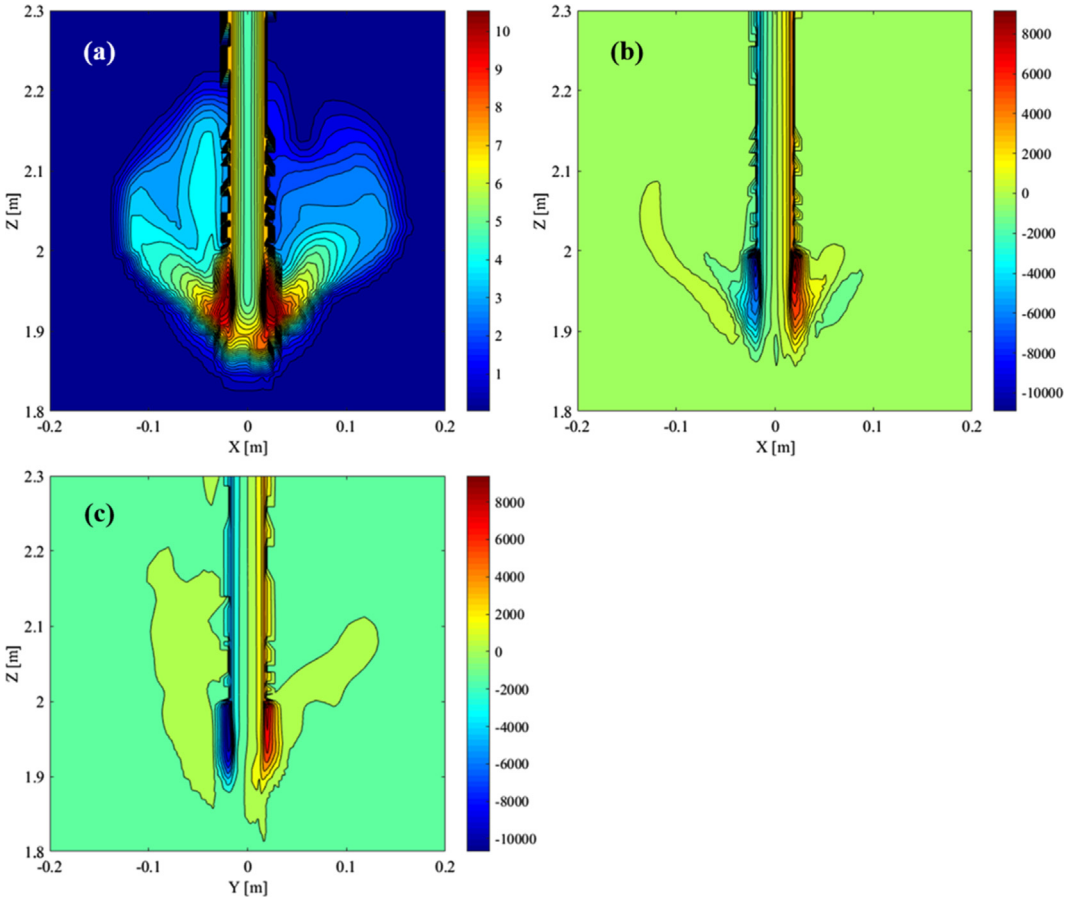

Fig. 15. Instantaneous quantities (a) Turbulent intensity; (b) du_z/dx; (c) du_z/dy in the lance region (l = 1.0 m).

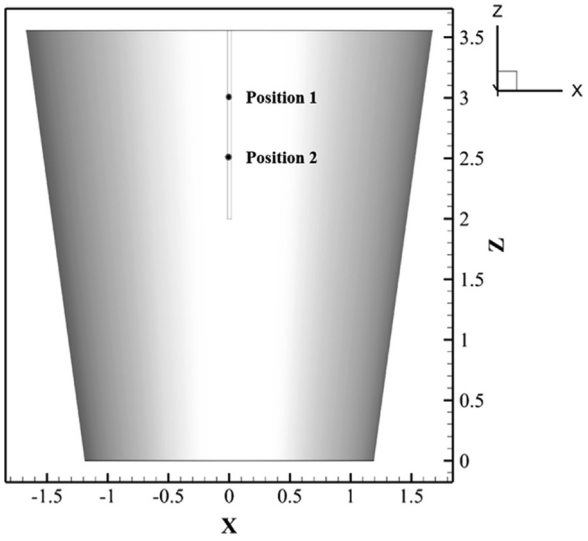

Fig. 16. Two positions for monitoring the pressure signal.

3.2.4. Surface sloshing

Surface sloshing motion is connected to vessel vibration and it affects the process quality such as melt loss and materials mixing in practice (Lamb, 1932). In order to clarify this surface sloshing effect by simulation, three positions are set at the gas-liquid interface to monitor the gas volume fraction α_g. The coordinates of the three positions are (−0.56 m, 0 m, 3.0 m), (0.56 m, 0 m, 3.0 m) and (−1.12 m, 0 m, 3.0 m), respectively. Positions 1 and 2 are symmetrical to the central axis, and they are closer to the central axis than position 3. The extent of the surface sloshing can be monitored by simulating change of gas volume fraction with time at the different positions. Fig. 18 shows a clear wave form for the evolution of the monitored gas volume fraction at the three different positions, even though the wave crests and troughs are not regular in some cases, especially for positions 1 and 2. The latter is probably because positions 1 and 2 are close to the gas plume region, where the monitored values of the gas volume fraction are affected by the escaping gas bubbles. The discrepancy of α_g between positions 1 and 2 suggests an asymmetrical feature of the surface sloshing. On the other hand, the sloshing motion at position 3 is much more regular due to a larger distance away from the plume region. As seen in Fig. 18(b), (d), (e) and (f), the wave amplitude increases with time, suggesting a propagation of the surface sloshing. Taking the surface wave in Fig. 18(f) as an example, the wave amplitude slowly changes during the first 1.5 s, and then the change becomes lager, and finally reaches a steady state after 4 s. This wave propagation process includes three stages, *i.e.*, wave excitation, growth and stabilization. Less than 1.0 s of the wave excitation is observed at positions 1 and 2, while it takes around 2 s to initiate the surface sloshing at position 3. This is attributed to a smaller distance to the vibration source (*i.e.*, the gas plume zone) for positions 1 and 2. It is also worth mentioning that the α_g monitored at position 1 (Fig. 18(a)) and position 2 (Fig. 18(c)) was not recorded at the beginning like that monitored at position 3 (Fig. 18(e)). This is why the starting α_g values in these figures are not the same, and the excitation stage does not appear in Fig. 18(a) and (c). In this sloshing system, a swelling on the top of the plume zone occurs due to the uprising

Please cite this article as: Y. Wang, L. Cao, M. Vanierschot et al., Modelling of gas injection into a viscous liquid through a top-submerged lance, Chemical Engineering Science, https://doi.org/10.1016/j.ces.2019.115359

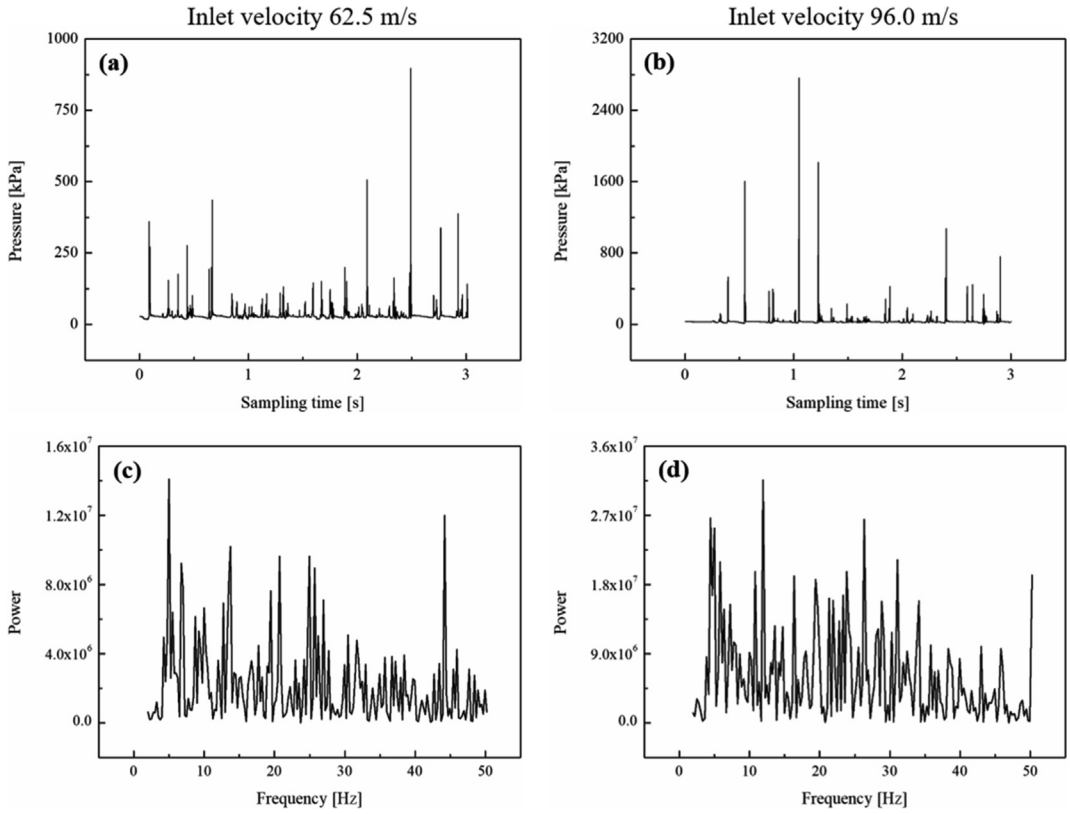

Fig. 17. Time trace of the averaged pressure signal ((a) and (b)) and its Fast Fourier Transform ((c) and (d)) (left column: inlet velocity 62.5 m/s; right column: inlet velocity 96.0 m/s) (l = 1.0 m).

gas bubbles, leading to an unbalanced pressure distribution along the surface. The pressure difference causes surface deformation and supplies energy for surface sloshing.

To further characterize the surface sloshing, the FFT technique is applied to deal with the recorded α_g values, and the results are shown in Fig. 19. A dominant frequency of around 0.9 Hz is detected in positions 1 and 2, and around 1.1 Hz in position 3. These monitored frequencies agree with the calculated values by Eq. (12) for surface sloshing (Lamb, 1932; Madarame et al., 2002), where the frequencies in the second and third modes are 0.89 Hz and 1.12 Hz, respectively. Based on the weak turbulence theory, the slope of the power-law frequency spectrum for gravity waves should be around −4 (Falcon et al., 2007). The slope ranges from −20/3 to −10/3 in our study, covering the value of −4, as demonstrated in Fig. 20. Since the Power Spectral Density (PSD) patterns generated at positions 1 and 2 are almost identical to that at position 3, only PSD pattern at position 3 is given in Fig. 20 to avoid a repetition. The surface sloshing is also monitored at position 3 with a 0.3 m lance depth. The corresponding wave amplitude (see Fig. 21(a)) is much smaller compared to that at the 1.0 m lance depth (see Fig. 18(f)). This is probably attributed to a less vigorous surface sloshing caused by a weaker buoyancy force when the submerged lance depth is decreased to 0.3 m. In spite of the pronounced variation of the surface amplitude, the sloshing frequency does not change considerably. The monitored frequency is also around 1.1 Hz, which corresponds to the frequency value in the third mode oscillation, 1.07 Hz, calculated from Eq. (12). This is consistent with the finding by Lee et al. (2003), where the wave motion was constant and only dependent on the vessel size when the liquid height or submerged depth is large enough. Since the sloshing wave becomes stable quickly, less than 4 s as shown in Fig. 18, only a part of the sampled data are presented to explain the sloshing wave propagation. Even though the total sampling time, namely, around 10 s may not be long enough for a statistical representation for the surface sloshing phenomena, it is much longer than the time needed for the sloshing wave being stabilized. In addition, compared the FFT frequencies with the theoretical values, a close agreement is obtained. Therefore, it is considered that the sampling time adopted in our work is reasonable.

$$f = \frac{1}{2\pi}\sqrt{\frac{k_i g}{R'}\tanh\left(\frac{k_i l}{R'}\right)} \quad (i = 1, 2, \cdots) \tag{12}$$

In the industrial situation, a rotary sloshing triggered by non-rotating surface waves generates a net angular momentum for the liquid (Schwarz, 1990). According to Hutton's work (Hutton, 1964), the maximum angular momentum of the liquid slag can be approximately evaluated by Eqs. (13) and (14). In Eq. (13), the value of wave amplitude, η_{max}, is considered as one-fifth of the averaged radius of the top and bottom radii of the slag pot. Therefore, the angular momentum is estimated to be around 4400 kg·m^2/s. Based on Eq. (15), the maximum velocity of the slag is calculated as 0.055 m/s during the sloshing. It was reported that even a velocity of 0.05 m/s could significantly decrease the mixing time (Schwarz, 1990). Therefore, this magnitude of angular momentum is likely to facilitate the mixing in the slag stabilization process.

$$M_l < 0.8\left(\frac{\eta_{max}}{a}\right)^2 M_o \tag{13}$$

$$M_o = \frac{\pi}{2}\rho_l a^4 \omega l \tag{14}$$

$$M_l = amu_l \tag{15}$$

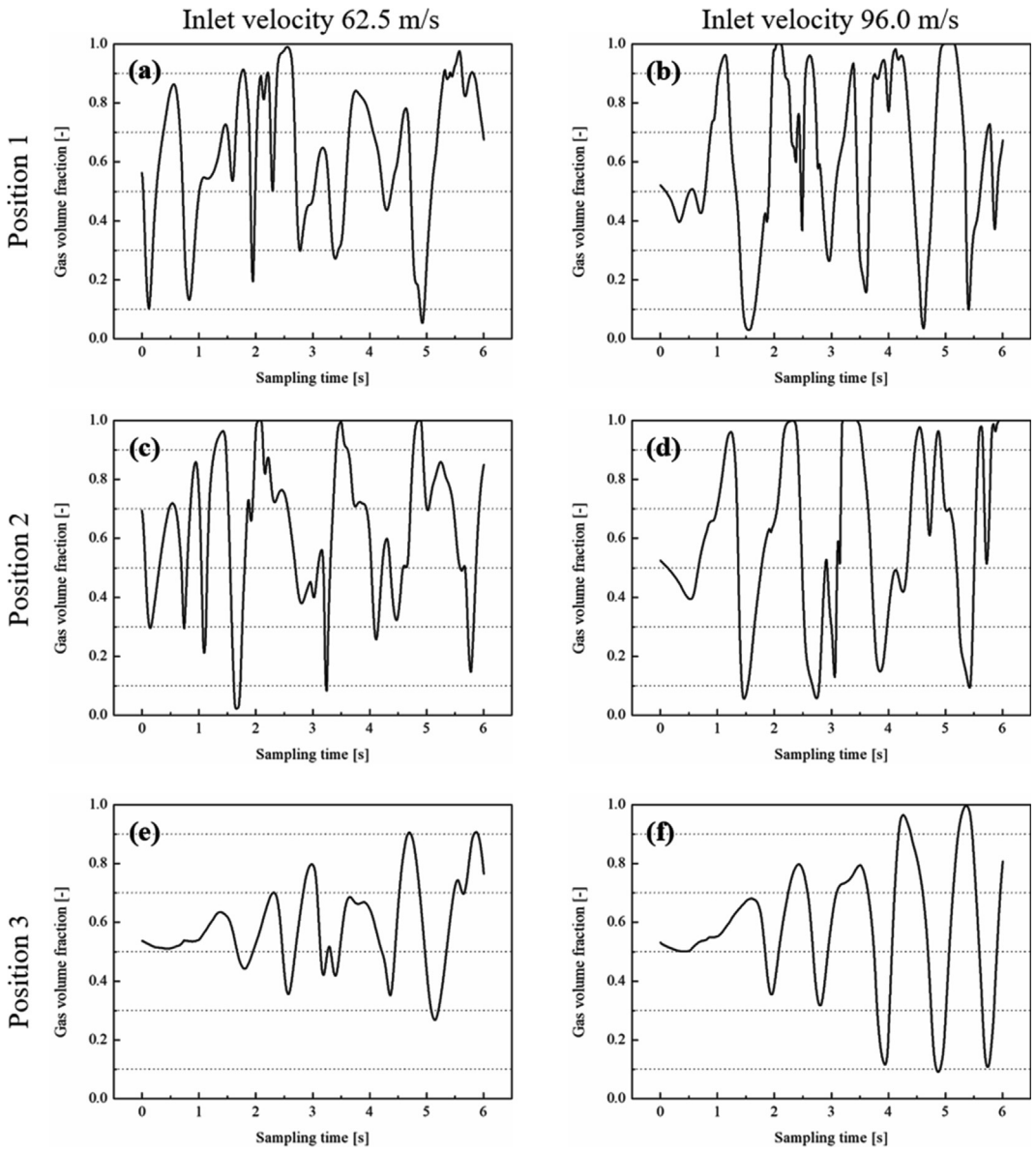

Fig. 18. Variation of gas volume fraction at monitoring points under two gas velocities (l = 1.0 m, position 1 ((−0.56 m, 0 m, 3.0 m), position 2 (0.56 m, 0 m, 3.0 m), position 3 (−1.12 m, 0 m, 3.0 m)).

3.2.5. Splashing

Splashing occurs in the slag stabilization process, resulting in not only operational difficulty but also serious oxidation of the metallic iron in the slag due to the fact that splashing causes an exposure of the entrained metallic iron phase to air. This affects metal recovery after the slag stabilization treatment. In such context, the splashing during the slag stabilization process has been mathematically simulated in the present work to clarify its mechanisms for the process optimization. Fig. 22 shows the splashing induced by shearing (Fig. 22(a) and (b)) and rupturing (Fig. 22(c) and (d)) under the conditions with lance depth of 1.0 m and inlet velocity of 96.0 m/s. As shown in Fig. 22(a), a gas bubble reaches the liquid surface at 2.1 s after the gas injection, and it tries to break through the surface, where a liquid slag film covering the gas bubble is generated due to the surface tension force. As the uprising of gas bubble continues, the liquid slag film on the top of the bubble surface becomes thin and the film breaks eventually, followed by its falling off along the bubble surface due to the gravity force. This backward movement generates a shear stress at the gas-liquid interface. The shear stress pulls down the liquid film from the rising gas bubble and shapes it into a fingerlike jet. Finally, this liquid finger becomes thin enough to break up, resulting in a splashing at 2.8 s, as demonstrated in Fig. 22(b). On the other hand, as the gas bubble passes through the interface, a liquid film wraps the gas bubble as observed at 2.46 s in Fig. 22(c). At 2.54 s, however, the liquid film ruptures due to the surface instability instead of shearing to a thinner one, leading to a splashing (Fig. 22(d)).

Slag splashing rate r is defined in Eq. (16). In order to quantitatively analyze the slag splashing behavior, the slag splashing rate is correlated with the input energy including the power due to gas kinetic energy, the work of the buoyancy force and bubble expansion. The input energy flux is calculated by Equation (17) (Schwarz, 1991). The energy efficiencies, η_1 and η_2, are both adopted as 0.06 (Lehrer, 1968; Wei et al., 1999). Fig. 23 shows a linear relationship between the splashing rate and the input energy flux at different operational conditions. This relationship is expressed by a semi-empirical equation (see Eq. (19)), based on which the slag splash-

Please cite this article as: Y. Wang, L. Cao, M. Vanierschot et al., Modelling of gas injection into a viscous liquid through a top-submerged lance, Chemical Engineering Science, https://doi.org/10.1016/j.ces.2019.115359

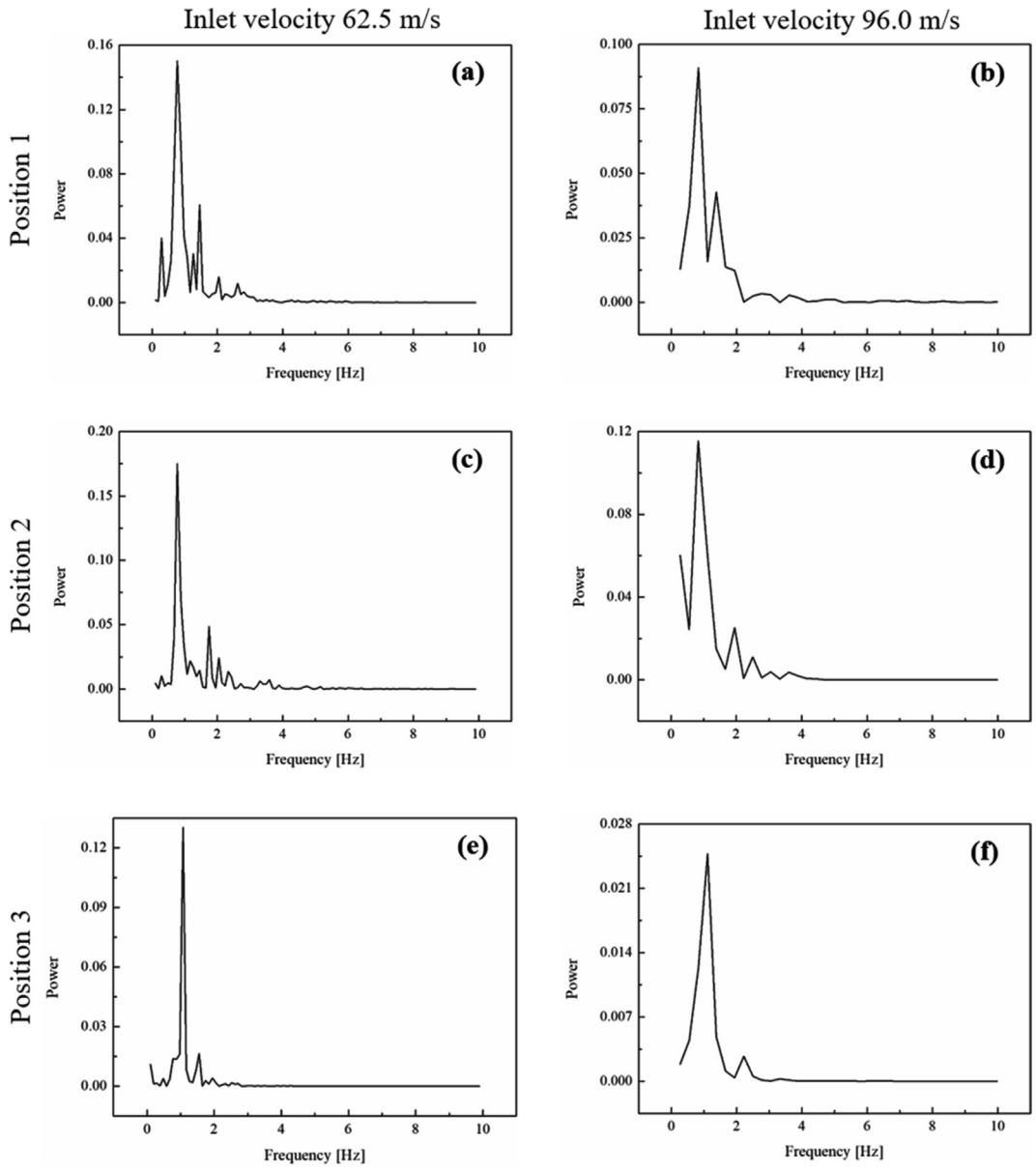

Fig. 19. Fast Fourier Transform of the monitored gas volume fraction (l = 1.0 m, position 1 ((−0.56 m, 0 m, 3.0 m), position 2 (0.56 m, 0 m, 3.0 m), position 3 (−1.12 m, 0 m, 3.0 m)).

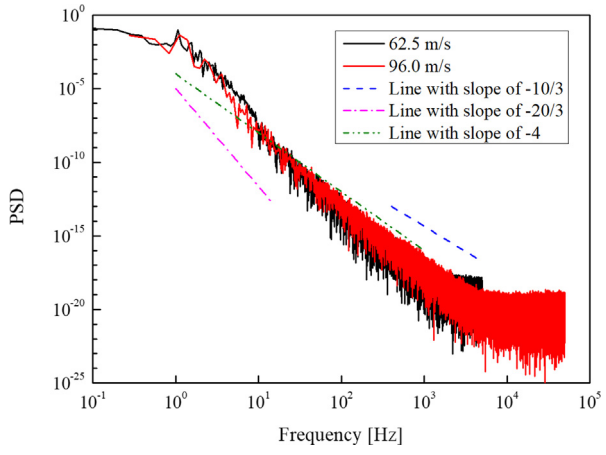

Fig. 20. Power spectral density of the monitored gas volume fraction at position 3 (−1.12 m, 0 m, 3.0 m) (l = 1.0 m).

ing can be effectively controlled by adjusting the operational conditions, therefore minimizing metal losses in the slag stabilization process.

$$r = \frac{\Delta m}{Vt} \tag{16}$$

$$E_{ln} = \left\{ Q_a p_a \left[2\ln\left(1 + \frac{\rho_l g l}{p_a}\right) - \frac{\rho_l g l}{p_a + \rho_l g l} \right] + \eta_1 E_{ke} + \eta_2 \dot{n} R (T_s - T_{in}) \frac{\rho_l g l}{p_a + \rho_l g l} \right\} / A \tag{17}$$

$$E_{ke} = \frac{1}{2} Q_a \rho_g u_g^2 \tag{18}$$

$$r = 3.456 \times 10^{-4} E_{ln} - 0.478 \tag{19}$$

3.2.6. Coherent structure

It has been discovered that the large-scale organized vortical motions, the Coherent Structures (CS), dominate heat, mass and

Please cite this article as: Y. Wang, L. Cao, M. Vanierschot et al., Modelling of gas injection into a viscous liquid through a top-submerged lance, Chemical Engineering Science, https://doi.org/10.1016/j.ces.2019.115359

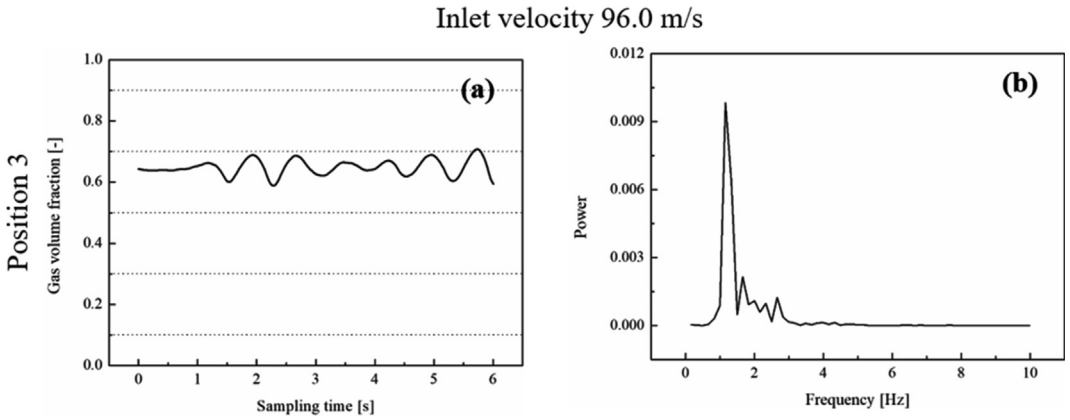

Fig. 21. Variation of gas volume fraction at position 3 (−1.12 m, 0 m, 3.0 m) and its Fast Fourier Transform (l = 0.3 m).

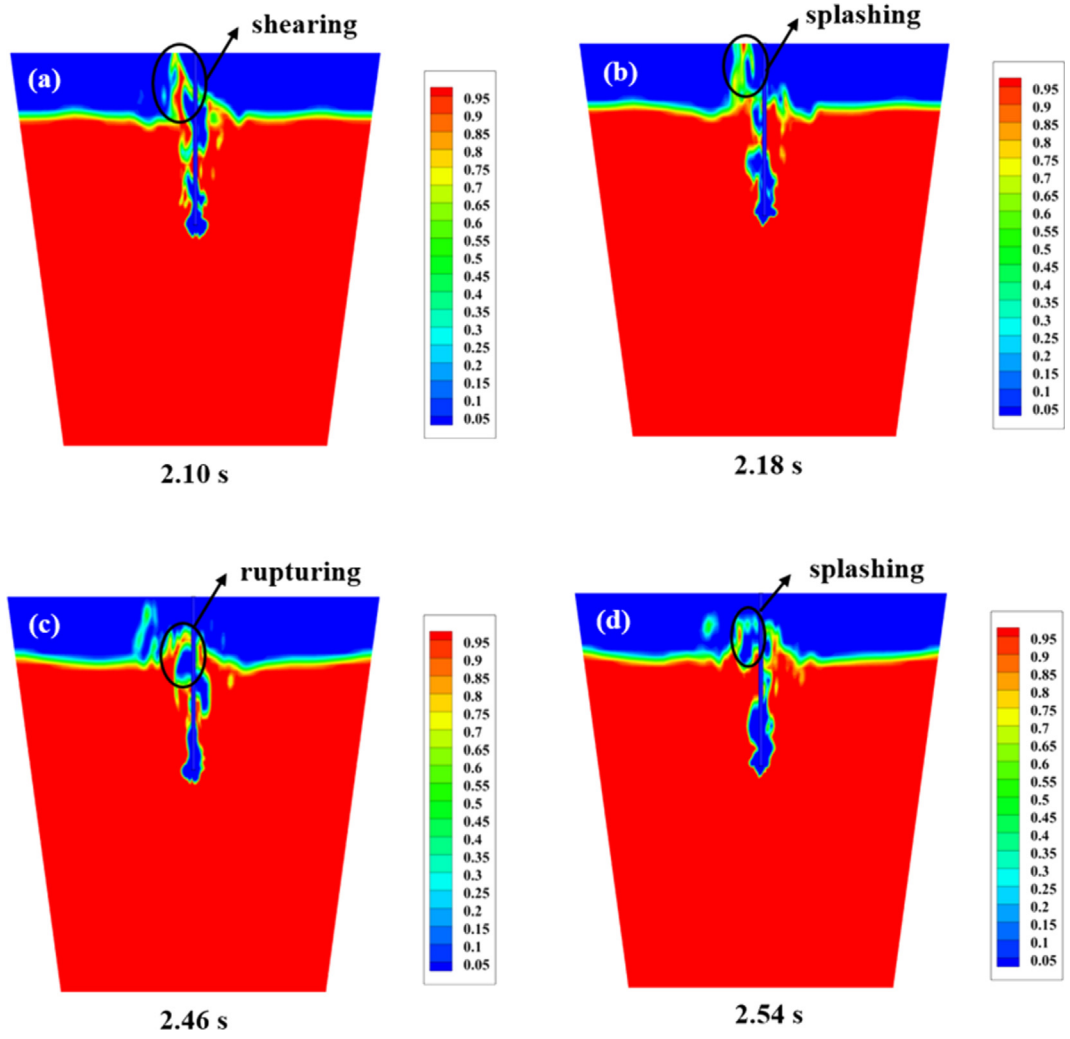

Fig. 22. Shearing and rupturing induced splashing (l = 1.0 m; inlet velocity = 96.0 m/s).

momentum transfer and chemical reactions in turbulent flow systems (Hussain et al., 1987; Hussain and Melander, 1991). There are several ways to extract CS from flows (Hunt et al., 1988; Chong et al., 1990; Jeong and Hussain, 1995). In this work, the -λ_2 approach is adopted for the top injection flow due to its accurate CS identification (Jeong and Hussain, 1995; Fulgosi et al., 2003; Liovic and Lakehal, 2007). Fig. 24(a) shows the *iso*-surface visualization of CS with the gas phase at the lance tip. The red surface indicates λ_2 = -2, and the translucent surface is the bubble surface represented by α_g = 0.5. It is obvious that the CS of this top injection flow is concentrated in the bubbly region due to the intensive eddy caused by the swirling bubbles with a fast rising velocity. The

Please cite this article as: Y. Wang, L. Cao, M. Vanierschot et al., Modelling of gas injection into a viscous liquid through a top-submerged lance, Chemical Engineering Science, https://doi.org/10.1016/j.ces.2019.115359

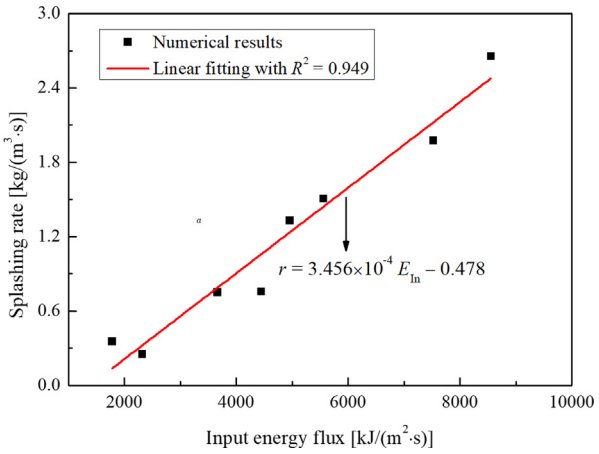

Fig. 23. Relationship between the slag splashing rate and the input energy flux.

swirling behavior of the bubble induced by the bubble oscillation can be observed from the bubble surface. The CS shape agrees with the bubble flow trajectory and seems like a mushroom-cloud. In addition, the hairpin vortices, one of the well-known CS features, are clearly identified. Fig. 24(b) and (c) show the CS feature of this top injection flow at l = 1.0 m and l = 0.3 m, respectively. It was found that the CS mainly appears in the top part of the slag pot, suggesting a strong vorticity in that region. This is in line with the feature of a buoyancy-driven top injection flow. Moreover, the CS of the flow at l = 1.0 m is much denser than that of flow at l = 0.3 m. This manifests a vigorous agitation at l = 1.0 m, which is beneficial to the additives mixing in the slag stabilization process. The mixing effect can be enhanced by increasing the submerged lance depth. The quantitative description of additives mixing as a function of submerged lance depth will be included in our future work. It is also worth mentioning that increasing the submerged lance depth will result in a large splashing rate. Therefore, in the slag stabilization process the submerged lance depth should be optimized by considering both the additive mixing and the slag splashing.

4. Conclusions

The model combination (*i.e.*, the VOF-RNG/LES model) is validated by PIV measurements for a Top Submerged Lance (TSL) injection flow. The flow characteristics of a TSL process are investigated by using the verified model combination under industrially relevant conditions. The main conclusions are summarized as follows:

(1) The averaged flow feature is captured by both the VOF-RNG/LES models, however, only the LES model successfully predicts the flow velocity fluctuation. The DSL SGS model slightly outperforms the WALE SGS model. Compared to the axial velocity component, the radial velocity component is more difficult to be predicted. It was found that 3D simulation is indispensable for modelling flow turbulence after a 2D *vs* 3D study.

(2) A semi-empirical equation is obtained to correlate the gas penetration depth into the molten slag with the modified Froude number. An intensive shear-induced turbulence is predicted near the lance tip due to a rapid decrease in the

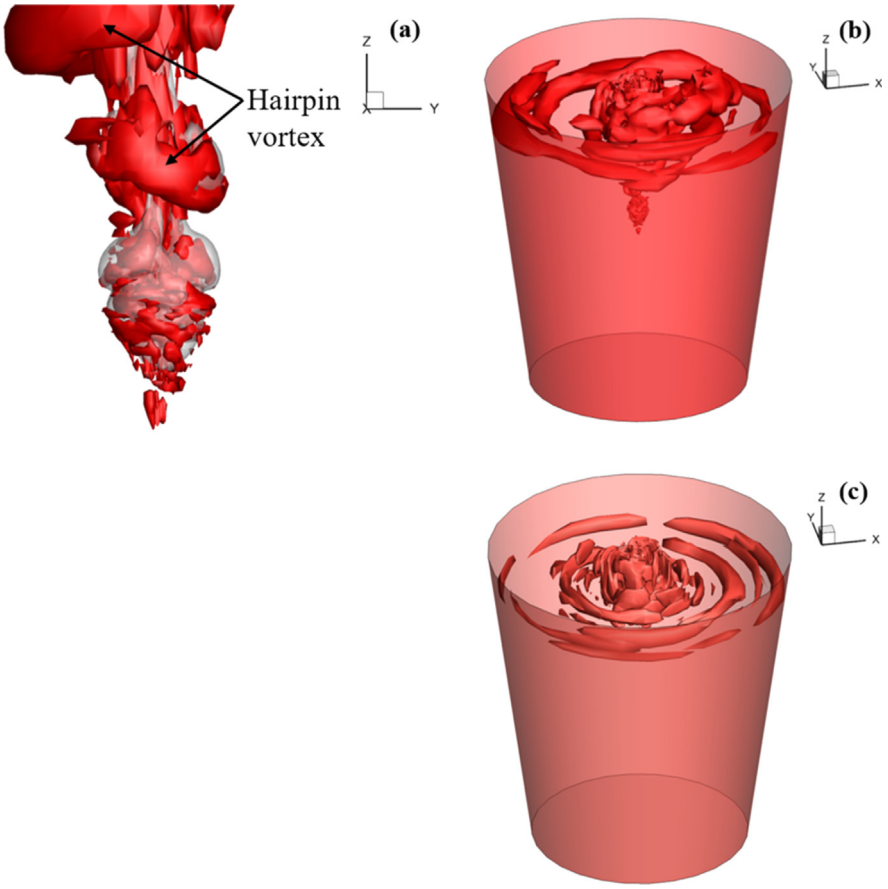

Fig. 24. Coherent structures at t = 6.5 s: (a) and (b) l = 1.0 m, (c) l = 0.3 m (inlet velocity = 96.0 m/s).

Please cite this article as: Y. Wang, L. Cao, M. Vanierschot et al., Modelling of gas injection into a viscous liquid through a top-submerged lance, Chemical Engineering Science, https://doi.org/10.1016/j.ces.2019.115359

gas velocity. Based on the recorded pressure and its FFT results, a pulsing jetting flow regime is detected, which would facilitate the additives mixing in the slag stabilization process. The sloshing propagation process consists of three stages, namely, excitation, growth and stabilization. It was proved that the wave amplitude of the sloshing changes with the submerged lance depth, whereas the wave frequency is constant at distinct lance depth. The surface sloshing generates a net angular momentum of 4400 kg·m^2/s, facilitating additives mixing in the slag pot. Two splashing mechanisms, *i.e.*, a shearing induced and a rupturing induced mechanism, are proposed to understand the splashing behavior under industrial conditions. The slag splashing rate is quantitatively correlated with the input energy flux of the system during the slag stabilization process. Coherent structures are identified in the top part of the slag pot, suggesting strong vortices in that region.

(3) The numerical results obtained by the developed 3D VOF-LES model can help the industrial operators to expand their insight in the flow behavior and lead to optimizing the slag stabilization process.

Author contributions

Yannan Wang participated in the PIV experiments, performed the simulations, analyzed the data and wrote this manuscript. Lingling Cao participated in the PIV experiments, made contributions to the discussion and reviewed the manuscript. Maarten Vanierschot performed the PIV experiments, helped interpret the results and reviewed the manuscript. Zhongfu Cheng, Bart Blanpain and Muxing Guo assisted in discussing the results and reviewing the manuscript.

Declaration of Competing Interest

The authors declare that they have no known competing financial interests or personal relationships that could have appeared to influence the work reported in this paper.

Acknowledgement

The authors gratefully acknowledge the computational support from HPC (KU Leuven) and financial support from Grant IWT project 140514 (Flanders). Yannan Wang and Lingling Cao also would like to express their gratitude to the China Scholarship Council (CSC). Yannan Wang thank Daniele Obiso from TU Freiberg for his helpful suggestion in computing the time-averaged velocity of the liquid phase in the VOF model.

Appendix A

Calculation of the Modified Froude number is listed below:

$$PV = nRT \tag{A1}$$

where P, V, n, R and T indicate gas pressure (Pa), gas volume per unit time or gas flow rate (m^3/s), amount of the gas (mol), gas constant (8.314 J·mol^{-1}·K^{-1}) and gas temperature (K), respectively. According to the idea gas law (Eq. (A1)), the gas flow rate at the operating conditions is obtained, as shown in Equation (A2):

$$V_2 = \frac{P_n V_n T_o}{P_o T_n} \tag{A2}$$

where the subscript n and o indicate the normal temperature and pressure condition and the operating temperature and pressure condition, respectively. The inlet gas velocity is then obtained through Eq. (A3). By substituting the inlet velocity and other relevant parameters in Eq. (9), the Modified Froude number is calculated as around 0.06 by considering the gas density of 1.225 kg/m^3 and characteristic length of 0.088 m in Eq. (9).

$$u_g = \frac{4P_n V_n T_o}{\pi P_o T_n d^2} \tag{A3}$$

References

ANSYS Inc., Ansys Theory Guide 16.2, 2015.
Brackbill, J.U., Kothe, D.B., Zemach, C., 1992. A continuum method for modeling surface tension. J. Comput. Phys. 100, 335–354.
Brigham, E.O., 1988. The Fast Fourier Transform and its Applications. Prentice Hall, New Jersey.
Chong, M.S., Perry, A.E., Cantwell, B.J., 1990. A general classification of three-dimensional flow fields. Phys. Fluids A 2, 765–777.
Cooley, J.W., Lewis, P.A.W., Welch, P.D., 1969. The fast Fourier transform and its application. IEEE Trans. Educ. 12, 27–34.
Crowe, C.T., Troutt, T.R., Chung, J.N., 1996. Numerical models for two-phase turbulent flows. Annu. Rev. Fluid. Mech. 28, 11–43.
Dippenaar, R., 2005. Industrial uses of slag (the use and re-use of iron and steelmaking slags). Ironmak. Steelmak. 32, 35–46.
Euroslag, www.euroslag.com (accessed on April 20, 2019).
Falcon, E., Laroche, C., Fauve, S., 2007. Observation of gravity-capillary wave turbulence. Phys. Rev. Lett. 98, 094503–094506.
Fulgosi, M., Lakehal, D., Banerjee, S., De Angelis, V., 2003. Direct numerical simulation of turbulence in a sheared air-water flow with a deformable interface. J. Fluid Mech. 482, 319–345.
Germano, M., Piomelli, U., Moin, P., Cabot, W.H., 1991. A dynamic subgrid-scale eddy viscosity model. Phys. Fluids A 3, 1760–1765.
Hoefele, E.O., Brimacombe, J.K., 1979. Flow regimes in submerged gas injection. Metall. Trans. B, 631–648.
Hou, Q., Zou, Z., 2005. Comparison between standard and renormalization group k-ε models in numerical simulation of swirling flow tundish. ISIJ Int. 45, 325–330.
Huda, N., Naser, J., Brooks, G., Reuter, M.A., Matusewicz, R.W., 2010. CFD modeling of swirl and nonswirl gas injection into liquid baths using top submerged lances. Metall. Mater. Trans. B 41B, 35–50.
Huda, N., Naser, J., Brooks, G., Reuter, M.A., Matusewicz, R.W., 2012. Computational fluid dynamic modeling of zinc slag fuming process in top-submerged lance smelting furnace. Metall. Mater. Trans. B 43B, 39–55.
Hunt, J.C.R., Wray, A.A., Moin, P., 1988. Eddies, streams, and convergence zones in turbulent flows. Proc. CTR Summer Program, 193–208.
Hussain, F., Husain, H., 1987. Passive and active control of jet turbulence. In: Liepman, H., Narasimha, R. (Eds.), Turbulence Management and Relaminarization. Springer, Verlag, New-York, Heidelberg, Berlin, pp. 445–457.
Hussain, F., Melander, M.V., 1991. Understanding turbulence via vortex dynamics. In: The Lumley Symposium: Studies in Turbulence. Springer, pp. 157–178.
Hutton, R.E., 1964. Fluid-particle motion during rotary sloshing. J. Appl. Mech. 31, 123–130.
Iguchi, M., Uemura, T., Yamaguchi, H., Kuranaga, T., Morita, Z., 1994. Fluid flow phenomena in a cylindrical bath agitated by top lance gas injection. ISIJ Int. 34, 973–979.
Igwe, B.U.N., Ramachandran, S., Fulton, J.C., 1973. Jet penetration and liquid splash in submerged gas injection. Metall. Trans. 4, 1887–1894.
Jeong, J., Hussain, F., 1995. On the identification of a vortex. J. Fluid Mech. 285, 69–94.
Jha, P.K., Ranjan, R., Mondal, S.S., Dash, S.K., 2003. Mixing in a tundish and a choice of turbulence model for its prediction. Int. J. Numer. Method H 13, 964–996.
Lakehal, Djamel, Smith, Brian L., Milelli, Massimo, 2002. Large-eddy simulation of bubbly turbulent shear flows. J. Turb. 3, N25. https://doi.org/10.1088/1468-5248/3/1/025.
Lamb, H., 1932. Hydrodynamics. Dover, New York.
Launder, B.E., Spalding, D.B., 1974. The numerical computation of turbulent flows. Comp. Meth. Appl. Mech. Eng. 3, 269–289.
Lee, M.S., O'Rourke, S.L., Molloy, N.A., 2003. Oscillatory flow in the steelmaking vessel. Scan. J. Metall. 32, 281–288.
Lehrer, L.H., 1968. Gas agitation of liquids. I & EC Process Design Dev. 7, 226–239.
Lilly, D.K., 1992. A proposed modification of the Germano subgrid-scale closure method. Phys. Fluids A 4, 633–635.
Liovic, P., Lakehal, D., 2007. Interface-turbulence interaction in large-scale bubbling processes. Int. J. Heat Fluid Flow 28, 127–144.
Liovic, P., Rudman, M., Liow, J.L., 2002. Numerical modelling of free surface flows in metallurgical vessels. Appl. Math. Modell. 26, 113–140.
Madarame, H., Okamoto, K., Iida, M., 2002. Self-induced sloshing caused by an upward round jet impinging on the free surface. J. Fluids Struct. 16, 417–433.
Mazumdar, D., Guthrie, R.I.L., 1985. Hydrodynamic modeling of some gas injection procedures in ladle metallurgy operations. Metall. Trans. B 16B, 83–90.
Mikhail, S.A., Turcotte, A.M., 1995. Thermal behaviour of basic oxygen furnace waste slag. Thermochim. Acta 263, 87–94.
Morsi, Y.S., Yang, W., Clayton, B.R., Gray, N.B., 2000. Experimental investigation of swirl and non-swirl gas injection into liquid baths using submerged vertical lances. Can. Metall. Quart. 39, 87–98.

Motz, H., Geiseler, J., 2001. Products of steel slags an opportunity to save natural resources. Waste Manage. 21, 285–293.
Nicoud, F., Ducros, F., 1999. Subgrid-scale stress modelling based on the square of the velocity gradient tensor. Flow Turbul. Combust. 62, 183–200.
Obiso, D., Kriebitzsch, S., Reuter, M., Meyer, B., 2019. The importance of viscous and interfacial forces in the hydrodynamics of the top-submerged-lance furnace. Metall. Mater. Trans. B 50B, 2403–2420.
Pan, Y., Langberg, D., 2010. Two-dimensional physical and CFD modelling of large gas bubble behavior in bath smelting furnaces. J. Comp. Multi Flows 2, 151–164.
Ruzicka, M.C., Drahos, J., Zahradnik, J., Thomas, N.H., 1997. Intermittent transition from bubbling to jetting regime in gas-liquid two phase flows. Int. J. Multiphase Flow 23, 671–682.
Santos, R.M., Ling, D., Sarvaramini, A., Guo, M., Elsen, J., Larachi, F., Beaudoin, G., Blanpain, B., Van Gerven, T., 2012. Stabilization of basic oxygen furnace slag by hot-stage carbonation treatment. Chem. Eng. J. 203, 239–250.
Sattar, M.A., Naser, J., Brooks, G., 2014. Numerical simulation of slag foaming on bath smelting slag (CaO-SiO_2-Al_2O_3-FeO) with population balance modeling. Chem. Eng. Sci. 107, 165–180.
Schwarz, M.P., 1990. Sloshing waves formed in gas-agitated baths. Chem. Eng. Sci., 1765–1777
Schwarz, M.P., 1991. Buoyancy and expansion power in gas-agitated baths. ISIJ Int. 31, 947–951.
Schwarze, R., Obermeier, F., Janke, D., 2001. Numerical simulation of fluid flow and disperse phase behavior in continuous casting tundishes. Modell. Simul. Mater. Sci. Eng. 9, 279–287.
Singh, V., Kumar, J., Bhanu, C., Ajmani, S.K., Dash, S.K., 2007. Optimisation of the bottom tuyeres configuration for the BOF vessel using physical and mathematical modelling. ISIJ Int. 47, 1605–1612.
Smagorinsky, J., 1963. General circulation experiments with the primitive equations. Month Wea. Rev. 91, 99–165.
Sutherland, W., 1893. The viscosity of gases and molecular force. Philos. Mag. Ser. 5 (223), 507–531.
Van Doormaal, J.P., Raithby, G.D., 1984. Enhancements of the SIMPLE method for predicting incompressible fluid flows. Numer. Heat Transfer 7, 147–163.
Vanierschot, M., Verrijssen, T.A.J., Van Buggenhout, S., Hendrickx, M., Van den Bulck, E., 2014. Experimental and numerical analysis of an apparatus to apply controlled shear/elongation in fluid flows. Chem. Eng. Sci. 113, 88–94.
Wang, Y., Vanierschot, M., Cao, L., Cheng, Z., Blanpain, B., Guo, M., 2018. Hydrodynamics study of bubbly flow in a top-submerged lance vessel. Chem. Eng. Sci. 192, 1091–1104.
Wang, G., Wang, Y., Gao, Z., 2010. Use of steel slag as a granular material: volume expansion prediction and usability criteria. J. Hazard. Mater. 184, 555–560.
Wei, J.H., Ma, J.C., Fan, Y.Y., Yu, N., Yang, S.L., Xiang, S.H., Zhu, D.P., 1999. Water modelling study of fluid flow and mixing characteristics in bath during AOD process. Ironmak. Steelmak. 26, 363–371.
Yakhot, V., Orszag, S.A., 1986. Renormalization group analysis of turbulence. I. Basic theory. J. Sci. Comp. 1, 3–51.
Yang, H., Wolters, J., Pischke, P., Soltner, H., Eckert, S., Fröhlich, J., 2017. Improved collision modelling for liquid metal droplets in a copper slag cleaning process. In: 12th International Conference on CFD in Oil&Gas, Metallurgical and Process Industries, Trondheim, Norway, pp. 355–363.
Youngs, D.L., 1982. Time-dependent multi-material flow with large fluid distortion. Numer. Methods Fluid Dyn. 24 (2), 273–285.
Zhao, Y.-F., Irons, G.A., 1990. The breakup of bubbles into jets during submerged gas injection. Metall. Trans. B, 997–1003.
Zhao, H., Yin, P., Zhang, L., Wang, S., 2016. Water model experiments of multiphase mixing in the top-blown smelting process of copper concentrate. Int. J. Miner. Metall. Mater. 23, 1369–1376.
Zhao, H., Zhang, L., Yin, P., Wang, S., 2017. Bubble motion and gas-liquid mixing in metallurgical reactor with a top submerged lance. Int. J. Chem. React. Eng. 15, 1–12.

Please cite this article as: Y. Wang, L. Cao, M. Vanierschot et al., Modelling of gas injection into a viscous liquid through a top-submerged lance, Chemical Engineering Science, https://doi.org/10.1016/j.ces.2019.115359